THEORETICAL AND EXPERIMENTAL STUDIES

OF CONFINED VORTEX FLOW

THEORETICAL AND EXPERIMENTAL STUDIES

OF CONFINED VORTEX FLOW

A

THESIS

by

RAOUL FRANÇOIS REYDON, B.Sc.

Department of Chemical Engineering

McGill University

Under the Supervision of Dr. W.H. Gauvin

Submitted to the Faculty of Graduate Studies
and Research of McGill University in partial
fulfilment of the requirements for the
degree of Master of Engineering

McGill University
MONTREAL, Canada   March 1978

To Bia

ABSTRACT

A study of air flow characteristics is reported for a vortex chamber consisting of an upper cylindrical section 122 cm in diameter and 61 cm high, and of a lower conical section 108 cm high. Quantitative measurements were made with a five-channel pressure probe of the radial profiles of tangential and axial velocities, as a function of the inlet air velocity (4.9, 8.6 and 12.3 m/s) and of the axial distance from the top of the chamber. Measurements of the static pressure profiles were made simultaneously. Finally, the angle of flow of the air entering through the single tangential inlet could be adjusted, and its effects on the flow recorded.

From these quantitative results and from a theoretical derivation based on the Navier-Stokes and the Continuity equations, generalized expressions for the tangential velocity profiles were obtained for the two regions of flow, forced-vortex and quasi-free vortex, which prevail in a confined vortex chamber, as a function of the entrance air velocity and of the radius at the point considered only. Surprisingly, the angle of entering air was found to have no effect on the tangential velocity, and only a minor effect on the static pressure distribution. On the other hand, the outlet diameter of the chamber was found to have a large effect on the profile of the axial velocities.

RÉSUMÉ

Une étude a été faite des caractéristiques d'un écoulement tourbillonaire dans une chambre expérimentale consistant d'une section supérieure cylindrique d'un diamètre de 122 cm et d'une hauteur de 61 cm, et d'une section inférieure conique mesurant 108 cm de haut. Des mesures quantitatives ont été faites avec une sonde de pression à cinq canaux des profils radiaux des vitesses tangentielles et axiales, en fonction de la vitesse d'arrivée de l'air (4.9, 8.6 et 12.3 m/s) et de la distance axiale mesurée en dessous du plafond de la chambre. Les profils de la pression statique ont été obtenus simultanément. Finalement, l'angle d'alimentation de l'air entrant dans la chambre a été varié et son effet sur l'écoulement a été observé.

A partir de ces données et aussi d'une étude théorique basée sur les équations de Navier-Stokes et de la Continuité, des expressions d'ordre général ont été dérivées pour les profils de vitesse tangentielles pour les deux régions d'écoulement (vortex forcé et vortex quasi-libre), en fonction de la vitesse de l'air entrant dans la chambre et du rayon au point considéré. Il a été surprenant d'observer que l'angle d'admission de l'air n'a aucun effet sur la vitesse tangentielle et seulement un effet mineur sur le profil des pressions statiques. D'autre part, le diamètre de la sortie de la partie conique de la chambre exerce une grande influence sur le profil des vitesses axiales.

iii

ACKNOWLEDGEMENTS

The author wishes to express his gratitude to all those who contributed to this work.

To his fellow graduate students, Mr. T. Mehmetoglu and Mr. O. Biceroglu, for their help in various stages of the investigation and many fruitful discussions.

To the professors and other students of the Chemical Engineering Department for discussions and valuable suggestions.

To the staff of the Chemical Engineering workshop for the construction of the equipment.

To Mrs. B. Toivanen for her patience and excellent typing.

To Mr. I. Sabadin for the meticulous preparation of the figures.

To McGill University for the financial support during the time of this investigation.

To Promon Engenharia, Sao Paulo, Brazil, for their support and understanding.

To my family for their moral support and encouragement.

And most important to my wife, Beatriz, whose extraordinary help and encouragement made this work possible.

iv

TABLE OF CONTENTS

LITERATURE REVIEW

EXPERIMENTAL SECTION

LIST OF FIGURES

LIST OF FIGURES

LIST OF TABLES

GENERAL INTRODUCTION

GENERAL INTRODUCTION

Vortex flows constitute an important class of fluid motion characterized by large-scale rotation of the mean flow around an axis. In addition to their natural occurrence as atmospheric vortices ranging widely in size from small dust-devils to very large tornadoes and hurricanes, vortex flows are finding a constantly increasing range of applications in technical operations and processing equipment. In these applications, use is made of the ability of a vortex to promote mixing and dispersion, to improve the stability of jets or to separate substances of different specific gravity or physical characteristics. From this, it can be inferred that the major field of applications will be in heterogeneous systems, where the dispersed phase will consist of entrained droplets or solid particles. A vortex also offers the added advantage of a longer contacting path between the two phases, as compared with a straight axial flow.

In cyclone dust separators, for example, vortex flow is used to separate suspended particles or droplets from effluent or process streams. Among other technical applications in wide use are: spray-dryers (1, 2); processing equipment such as spray-coolers; gas scrubbers, absorbers, cyclone evaporators (3); centrifugal burners (4, 5); oil-water separators (6) and, more recently, plasma flame stabilization (7, 8, 9). The Ranque-Hilsch vortex tube is a unique

example of single-phase vortex motion, which causes much interest
in the refrigeration field (10).

In spite of the wide range of applications, the mechanics
of vortex flow are not completely understood, principally because
of the three-dimensional character of the motion and the complexity
introduced by the co-existence of two or more regimes of flow in
the same piece of equipment. In the past, investigations have been
largely concerned with the measurement of the gross behaviour of
the equipment such as pressure drop and separation efficiency.
Only a few analyses have considered variations of the geometric shape
of the confining equipment (11, 12) and many investigations have
oversimplified the complexities of the flow. It is only recently
that an effort has been initiated to obtain a better understanding
of the fundamental principles involved. From a practical point of
view, the prediction of the three-dimensional velocity profiles as
a function of the geometry of the vortex system and of the operating
conditions is probably the most important aspect of the design and
operation of the equipment in which vortex motion is used. These
profiles, in turn, dictate the flow pattern of the motion and the
general performance of the vortex system.

The present study constitutes a continuation of the work
initiated in this laboratory by Nader Bank (13, 14, 15). Using a
single hot-wire anemometer probe rotated in eight different az-
imuthal directions at a given position in the flow, for which
specific response equations had to be developed (14), Bank measured

the velocity profiles of an ambient temperature air vortex flow
generated in a chamber with a cylindrical top and a conical bottom.
His investigation was limited to low volumetric flow rates, not
exceeding 3.2 m/s in inlet velocity. Because of the poor response
of his measurement technique at very low velocities, he was not
able to make any measurement of the radial velocities and ex-
perienced serious restrictions in the determination of the axial
component at any except the higher velocities. On the other hand,
the use of a hot-wire anemometer probe permitted him to provide
interesting data on the radial distributions of tangential and
axial intensities of turbulence, which are among the first to be
published in this type of system.

, In the present study, use has been made of the same
chamber. However, the range of volumetric flow rates has been
greatly increased and provision has been made to control the inlet
flow angle, a parameter which Bank identified as of possible im-
portance. Another important departure from Bank's experimental
technique was the adoption of a three-dimensional five-channel
pressure probe as the measuring device, to improve the resolution
and simplicity in recording the velocities. More specifically, the
objectives of the investigations were:

  a) To study the variations of the velocity and
     static pressure fields as functions of the
     following parameters: gas flow rate, angle of
     inlet flow, and axial and radial position.

b) To attempt to derive from first principles a
correlation for the tangential velocity as a
function of the above parameters and to compare
this prediction with the experimentally-observed
values.

A great deal of effort was expended in the detailed
measurement of the tangential velocity profiles, in view of their
paramount importance in the design of process equipment.

This thesis is divided into two parts. The first part
consists of a Literature Review which has extended Bank's fairly
complete review of the prior literature to include some recent
additions to the body of experimental evidence. It also includes
a discussion of the more promising instrumental techniques avail-
able for the characterization of swirling motion.

In the second part, a report is presented of the exper-
imental investigation proper. This part of the thesis is written
in the format of a paper, and is complete in itself. This format,
so familiar to readers of the scientific literature, has been used
to facilitate the presentation, interpretation and comprehension of
the work.

LITERATURE REVIEW

INTRODUCTION

As stressed by many researchers (15, 16) vortex fluid flow is, by its very nature, three dimensional in character. This implies that the velocity vectors must be decomposed into their three components and the natural choice has been to use cylindrical coordinates to represent these components because of the axisymmetric pattern of the flow field. This approach has been taken by all authors whose works were surveyed here.

This survey is divided into two parts: the first deals with vortex flows and their properties, while the second covers the characteristics of the measuring probes which are most appropriate for swirl flow investigations.

As a fairly complete review of vortex flows has already been presented by N. Bank, which can be found in references (13, 15), only the more pertinent of past studies will be recalled here. In addition, reference will be made to recent work which has appeared in the published literature since the completion of Bank's investigation, as well as to some other studies not reported by Bank.

Whenever possible, comparison between the results of different investigators will be made, although this task is often rendered difficult by the different test geometries as well as conditions of operation which have been used.

VORTEX FLOWS

Marshall (1) described in 1954 the vortical velocity distribution for air flow in spray dryers. He noted the presence of a central forced vortex where the air rotates as a rigid body with zero velocity at the axis, surrounded by a free vortex in which the tangential velocity varies inversely with the radius. He also mentioned that the tangential velocities might be from ten to fifteen times higher than the axial velocities, and that these axial components had little real significance for computing particle motion.

In 1958, Rietema and Krajenbrink (17) presented a theoretical derivation of tangential velocity profiles in a flat box vortex chamber. The derivation of their expressions included the influence of eddy viscosity and of wall friction. The most important parameter controlling the tangential velocity profile was found to be

$$\lambda = -u_0 R/(v + \epsilon) \tag{1}$$

where u_0 is the radial velocity at the outer radius $\underline{R}$ of the vortex chamber, $\underline{v}$ is the kinematic viscosity and $\underline{\epsilon}$ is the kinematic eddy viscosity. For values of λ greater than about 10, the tangential velocity profile was found to be nearly hyperbolic, while for λ smaller than 1 the tangential velocity decreased towards the centre approximating a straight line dependence on the radius (solid body rotation).

Schowalter and Johnstone (18) measured flow variables in a

vortex tube and in a conventional cyclone separator. They showed that the sensitivity of the patterns of flow were small relative to changes in flow rate and were large relative to geometrical changes. They did not obtain a symmetric flow in either of the two system configurations. The tangential velocity profiles measured for the cyclone were roughly approximated by the theoretical distribution derived by Rietema and Krajenbrink (17) and observed before by Marshall (1) and others (15).

In 1962, Kendall (19) in his study of compressible viscous vortices stated that the shape of the tangential velocity distribution was controlled by the radial Reynolds number defined as $(Re)_r = ur/v$, where u and v are the radial velocity, and kinematic viscosity, respectively, and r is the radius. For very low Reynolds numbers, the tangential velocity was found to be proportional to the radius (solid-body rotation). As $(Re)_r$ increased, the velocity approached war^{-1} (vortex flow), except near the axis, where solid-body rotation always occurred. It should be noted that this radial Reynolds number is similar to Rietema and Krajenbrink's λ discussed before, but does not include the eddy viscosity.

Kendall also noted that two-dimensional models can fail to represent three-dimensional experiments unless turbulent shearing stresses are accounted for. As an example, he described in detail the behaviour of the flow near the top and bottom closures of a cylindrical chamber. On these two flat surfaces, there are very strong pressure gradients towards the axis right inside the two

boundary layers caused by the centrifugal forces in the main flow. Even though these layers are thin compared to the dimensions of a vortex chamber, he explained that the radial velocity within these layers is so much larger than that of the vortex that it could not be neglected as carrier of mass flow. Clearly, this situation cannot be accounted for by a two-dimensional model. Later, Kotas (20) performed experiments proving that fluid can enter and leave a flat box vortex chamber (a cylindrical chamber in which the tangential entry extends over the whole height of the chamber) without passing through the main part of the flow, being transported only in the boundary layers. Besides velocity measurements through the boundary layers, Kendall also performed static pressure measurements for the three cylindrical chambers he used in his experimental investigation, of which the largest was 6 in (15.24 cm) in diameter. One of these was rotated at very high speeds (up to 13,000 RPM).

In 1967, Baluev and Troyankin from the Moscow Power Institute published two papers (11, 12) dealing with the study of the aerodynamic structure of gas flow in a cyclone chamber and with the effect of the design parameters. Their investigation was mainly experimental. They obtained an empirical equation, derived from their experimental results, for the estimation of the tangential velocity over the radius and height of a cylindrical chamber, for various geometrical inlet and outlet configurations, and for various degrees of surface roughness. A 180-mm diameter cylindrical chamber was used, with air as fluid medium being injected tangentially near

the top and withdrawn at the bottom. The measurements were obtained with the aid of a calibrated five-hole probe. No other details about the measurement methods were given.

They noted the existence and the importance of secondary flows and their effect on the efficiency of the cyclone, and also reported a lack of symmetry relative to the cyclone axis. They showed that this asymmetry was larger for the axial velocity components, particularly near the exit. According to their results, it can be concluded that the cyclone volume contains a number of circulating vortex zones and reverse streams. The configuration of the tangential nozzles did not exert a decisive effect on the flow patterns, but the throat diameter (that is, the diameter of the exit pipe) was observed to be one of the main design parameters of the cyclone chamber, although they did not specify its effect.

They identified two main downward flows, rotating co-axially: the wall flow, and a stream located in the region where the maximum tangential velocity occurs. They also measured a stream going upwards at the axis of the chamber. The static pressure profiles were determined as having their maximum values near the confining walls and the minimum at the axis of the flow. These pressure profiles were shown to decrease drastically in the region of the maximum tangential velocities. Figure 1 shows a diagramatic representation of their results for their double tangential inlet chamber. The same authors continued their study in 1969 with an experimental paper on the aerodynamic resistance of a cylindrical

FIGURE 1

DIAGRAM WITH BALUEV'S RESULTS

FOR VORTEX FLOW PATTERNS
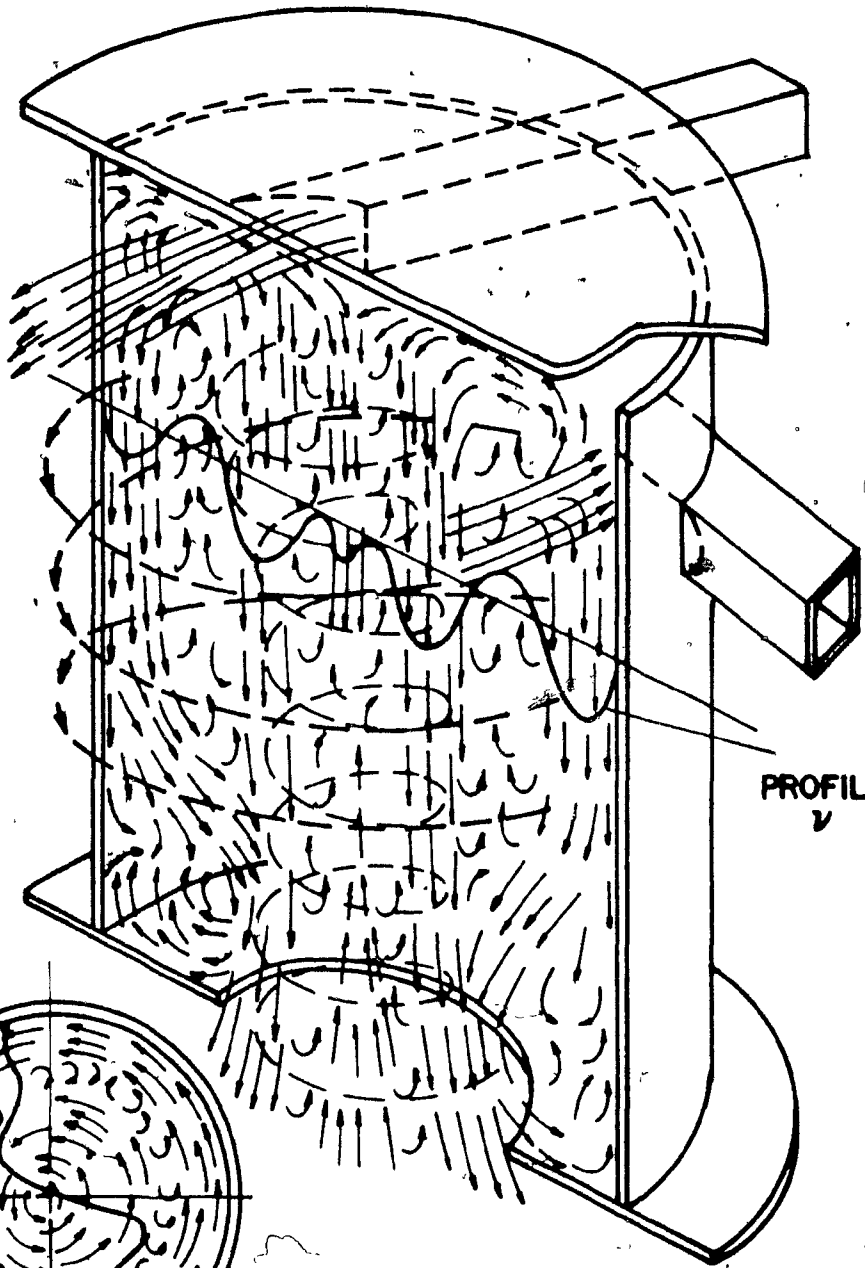
PROFILE
ν

PROFILE
ω
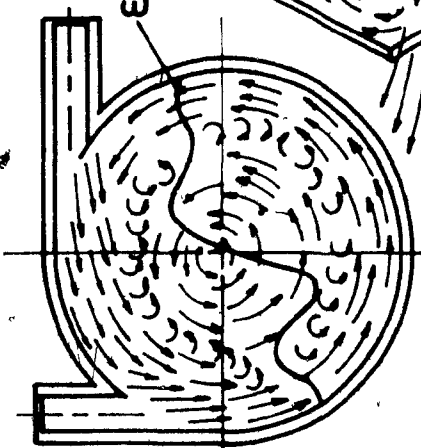
NOZZLE
SECTION

SECTION OVER CENTRE
PART OF CHAMBER

cyclone chamber (21).

In 1972 Koval and Mikhailov (4) published an investigation on the general equations of the dynamics of swirl flow for a real (viscous) liquid. They substituted the turbulent kinematic viscosity coefficient to the kinematic viscosity in the Navier-Stokes equations and, using also the continuity equation, they obtained general forms for the tangential velocity and static pressure profiles in various regions of the flow. Their conclusions concerning the form of the velocity profiles generally agreed with those reached by Baluev and Troyankin, Kendall, and Rietema and Krajenbrink. The equations for the regions of the flow other than the free vortex were derived on the basis of the maximum tangential velocity and its radial position as parameters. This approach considerably restricts the use of this type of equation in prediction models.

For the free vortex region, the tangential velocity profile was found to be given by:

$$w/w_R = (r/R)^{1-k} \qquad (2)$$

where $\underline{w}$ and $\underline{w}_R$ are the tangential velocities at radius $\underline{r}$ and at $\underline{R}$, the radius of the chamber, and $\underline{k}$ is of the same form as Kendall's $(Re)_r$ with, however, the eddy viscosity replacing the kinematic viscosity.

Syred and Beer (1974) in a study of the utilization of

swirling flows for combustion (5) explained that, because of their complexity, these flows are poorly understood. They stressed the importance of vortex motion for the improvement of flame stability as a result of the formation of toroidal recirculation zones and for the reduction of combustion lengths by producing fast mixing and high rates of entrainment of the ambient fluid. They noted that cyclone combustion chambers have large internal reverse flow zones which provide very long residence times for the fuel/air mixture and that they are well suited for the combustion of difficult materials, such as poor quality coal or vegetable refuse. They suggested that angling the tangential inlet jets could alter the direction of the flow and intensify it near the wall of the chamber.

In 1975, Ogawa published his work on the pressure drop through cyclone dust collectors (22) which also included measurements of velocity profiles performed with a pressure probe. These profiles were needed for the development of an equation for the pressure drop. The following year, Ogawa published a paper on the flow patterns of the turbulent rotational flow in the returned type of vortex chamber (23). Figure 2 shows this chamber's configuration. He recognized that the structure of the rotational flow is of a very complicated nature due to the action of the turbulent fluctuating velocity. He derived a theoretical equation for the tangential velocity, the static pressure and the eddy kinematic viscosity, starting from the continuity equation, Reynold's equation for turbulent rotational flow and the energy equation.

FIGURE 2

OGAWA'S RETURNED TYPE VORTEX CHAMBER

RETURNED TYPE VORTEX CHAMBER
USED BY OGAWA
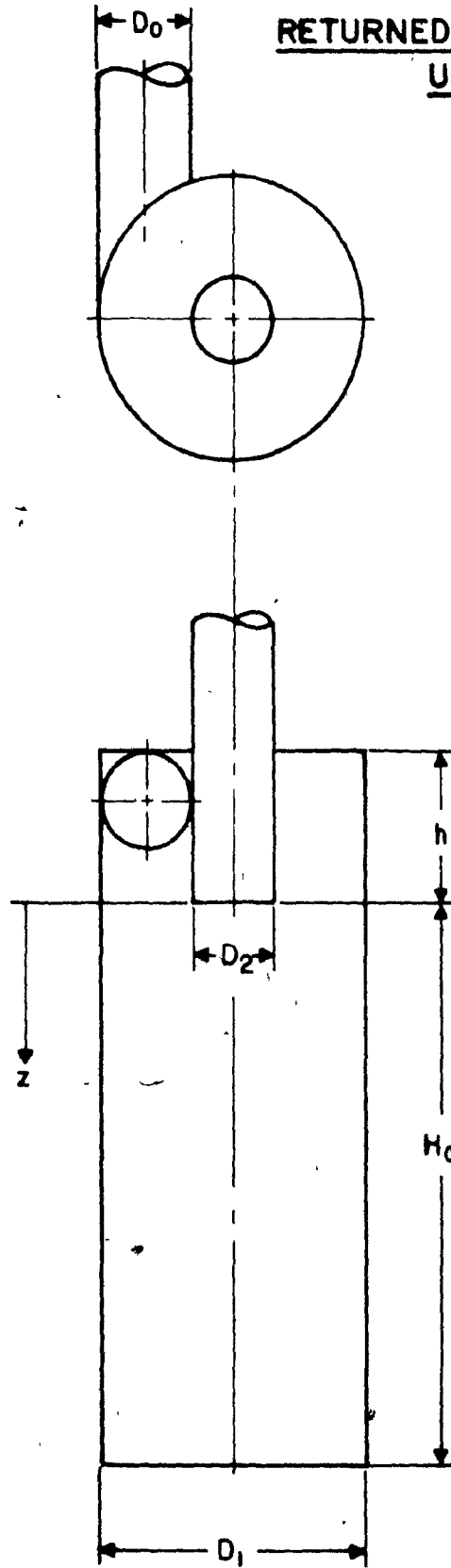
D_0 = 47.5 mm
D_1 = 140 mm
D_2 = 47.5 mm
H_0 = 295 mm
h = 80 mm

Ogawa compared his theoretical equation with experimental results obtained with a 3-mm diameter cylindrical pitot tube in a 140-mm diameter cylindrical returned type vortex chamber. The agreement was reasonable in spite of the many simplifications introduced in the course of the theoretical derivations. His results also agreed qualitatively with those reported by earlier investigators. No details were given for the measurement instrumentation.

Finally, in 1977 Ogawa published results on the motion of fine solid particles in the turbulent rotational flow (24). He derived equations from a balance of forces on a particle (centrifugal, drag and gravity) using velocity data obtained in his previous paper. These equations were compared with experimental results obtained by collecting particles with a small adhesive tape inserted in the flow at known positions. The agreement was fair.

SUMMARY

It has been shown that flow patterns exert a major effect on the efficiency of the operation of industrial equipment utilizing vortex flow.

Small attention has been given in the literature to vortex chamber geometries different from the cylindrical. Most of the investigations dealt with vortex tubes.

Many investigations not reported here were limited to

measurements and predictions of temperature and static pressure profiles based on assumed velocity fields.

Since the test geometries were generally different, with many details lacking, it is difficult to compare quantitatively the results of diverse researchers. In reference (15), Bank noted that adequate descriptions of the experimental apparatus and specifications of the instrumentation were generally not given by most authors, with the result that many published data are unduly biased owing to lack of complete information.

In a general sense, experimental and theoretical results of most workers agree in the following important characteristics of confined vortex flows, most of which were noted by Bank and Gauvin (13, 15):

a) The confined vortex flow pattern is three-dimensional in nature (4, 11, 12, 13, 15, 16, 23).

b) The tangential velocity component is predominant and the radial velocity component is very small in the entire vortex flow (1, 11, 12, 13, 15, 17, 18, 23).

c) An important downward axial flow occurs in the annular region adjacent to the wall (11, 12, 13, 15, 23). Some workers observed also a substantial axial flow in the maximum tangential velocity component region (11, 12).

d) The axial velocity may show a reversal near the axis of the vortex chamber (11, 12, 13, 15).

e) The tangential velocity component profile is composed mainly of two regions: a peripheral region of quasi-free vortex (where $wr = k_1$ is approximated) and a central region of quasi-forced vortex flow (where $w = k_2 r$ is approximated). $\underline{w}$ here is the tangential velocity component, $\underline{r}$ is the radius, $\underline{k_1}$ and $\underline{k_2}$ are constants (1, 11, 12, 17, 19).

f) In a vortex flow, there may be a helical-shape dynamic axis of symmetry (13, 15, 18).

g) It seems that the angle of inlet may change the axial flow pattern, mainly near the walls (5, 13, 15).

h) The static pressure is high near the vortex flow confining walls and decreases drastically near the axis, where it reaches its minimum (4, 19, 23).

This survey made it clear that more detailed measurements of the vortex flow characteristics, together with a sound theoretical analysis, are required to permit the elaboration of generalized expressions for the prediction of the component velocities, suitable for design purposes. Of these, the tangential velocity is by far the most important. Other geometries than cylindrical chambers should also be studied for the complete generalization of these prediction models, and careful attention should be devoted to the effect of the inlet flow angles.

MEASUREMENT TECHNIQUES IN VORTEX FLOWS

Visualizations of the flow for qualitative descriptions
of parts of the vortex flow field have been reported many times but
attempts to quantify these visual observations were rarely success-
ful.

Almost all the reported measurements of velocity patterns
are based upon the introduction of probes into the flow. In quite
a few cases the size of the probe relative to the dimensions of the
flow was not small enough to avoid instabilities and local disturb-
ances. However, accurate velocity measurements can be obtained if
the disturbing effects of the probe are minimized.

In this section of the literature survey, some of the more
promising techniques of measuring in the special case of swirling
flows will be reviewed, with particular emphasis on the five-channel
(three dimensional) directional pressure probe, which was the
instrument selected for the present study.

Hot Wire Anemometer

This device consists of one or more small electrically-
heated cylindrical wires whose rate of heat loss to the surrounding
fluid is a complex function of the local velocity. With the aid of
a suitable circuitry, the instantaneous velocity of the fluid can
be measured and serve as a means to calculate turbulence character-
istics and mean velocity components.

In Bank's case (15), for example, a wire 1.1-mm long of platinum-coated tungsten 0.005-mm in diameter, supported by nickel pins, was used. The body of the probe was 7-mm in diameter. As is common in this type of probe, the temperature of the wire is maintained constant.

For three dimensional flow fields the components of velocity have been determined by two methods: introduction of single wires and varying the orientation of the probe to the main flow direction, or introduction of a three-wire probe for which each wire requires a separate anemometer circuit. Bank used the former method (13) after deriving theoretically special response equations for it (14). More details and bibliography can be found in references (15) and (16).

The main differentiating characteristics of this measurement device is its high frequency response. In reference (13) mentioned above, the frequency response of the anemometer was always found to be such that its 3dB down point (roll-off frequency) was greater than 5Hz.

Arya and Plate (25) stated that as long as the fluctuating velocity component was smaller than about 20% of the local mean velocity, the measurements were reliable and turbulence measurements by means of hot-wire anemometer could be made. If there are also temperature fluctuations in the flow field, care must be taken to separate its effects on the hot-wire. Methods for this are also

described by Arya and Plate. Chevray and Tutu (26) stated that
constant-current hot-wire anemometers (as opposed to the constant-
temperature hot wires discussed so far) have been used to measure
mean as well as fluctuating velocities in non-isothermal flows,
albeit it is well known that the output from such a device is not
yet amenable to linearization.

Among other conditions for the reliability of the hot-
wire are (27): the wire temperature should be low enough to make
the highly non-linear radiation effect negligible; the length-to-
diameter ratio should be large enough so that end conduction can be
neglected; on the other hand, the shorter the wire, the better it
will sense the local variables. It was also concluded (28) that
the presence of a mean-velocity gradient along the length of a hot-
wire operated at constant temperature causes a skewed wire tem-
perature distribution which influences both the steady-state and the
dynamic responses of the wire. If a uniform flow calibration curve
is used to evaluate the local mean velocity at the centre of a wire
exposed to mean shear, some accuracy will be lost. By the same
token, frequent calibrations of voltage as function of velocity and
compensation for ambient temperature and density variation must be
made.

When comparing the features of a hot-wire anemometer with
those of a total-head tube, one finds that the former instrument
has better sensitivity at low velocities than the latter, which has
a response proportional to the square of velocity, while the hot-

wire response is approximately proportional to the square root of velocity. In addition, a liquid manometer, when used as an adjunct to the tube, cannot follow rapid pressure fluctuations and therefore cannot be used for measuring turbulent fluctuations.

The limitations of the hot-wire anemometer as a research tool for measuring velocity components are well documented (27), and are due partly to the transport phenomena involved, and to the high degree of instrumental complexity which most cases require to be employed.

Five-Channel Pressure Probe

The five-channel pressure probe, the instrument used in the present study, offers particular advantages for the measurement of mean flow characteristics, namely reasonably small size causing negligible disturbance when the confined flow is not too small, and the absence of complicated electronic circuitry. It is used to measure yaw and pitch angles, as well as total and static pressures. Five pressure tappings are distributed on a cylindrical tube. Various configurations have been proposed for these distributions and are compared by Bryer, Walsche and Garner (29). For the hemispherical type, one of the tappings is on the axis and the other four are spaced equidistant from the first, as shown in Figure 3. Figure 4 shows the cylindrical wedge-probe type which has been chosen for this study.

The principle of operation (16) of the probe is based upon

FIGURE 3

HEMISPHERICAL-TYPE FIVE-CHANNEL PRESSURE PROBE

# HEMISPHERICAL FIVE-HOLE PRESSURE PROBE
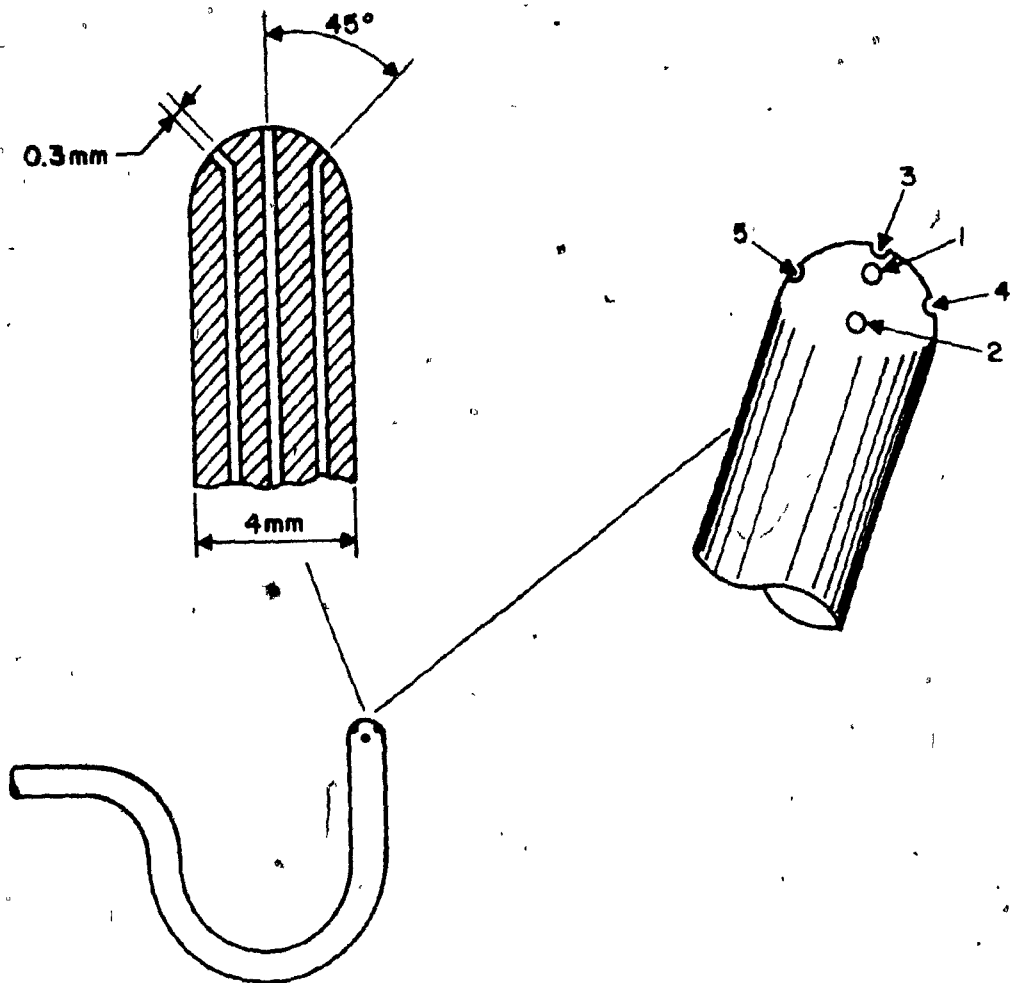
FIGURE 4

CYLINDRICAL-WEDGE-FIVE CHANNEL PRESSURE PROBE
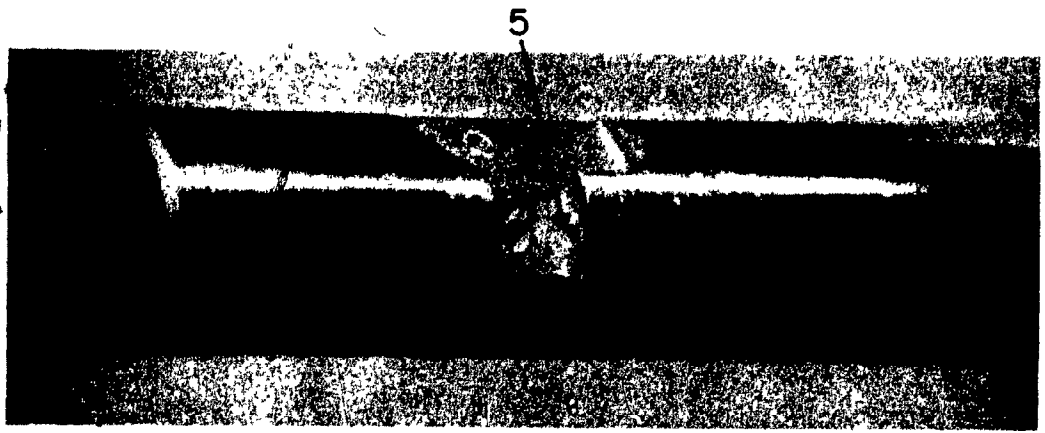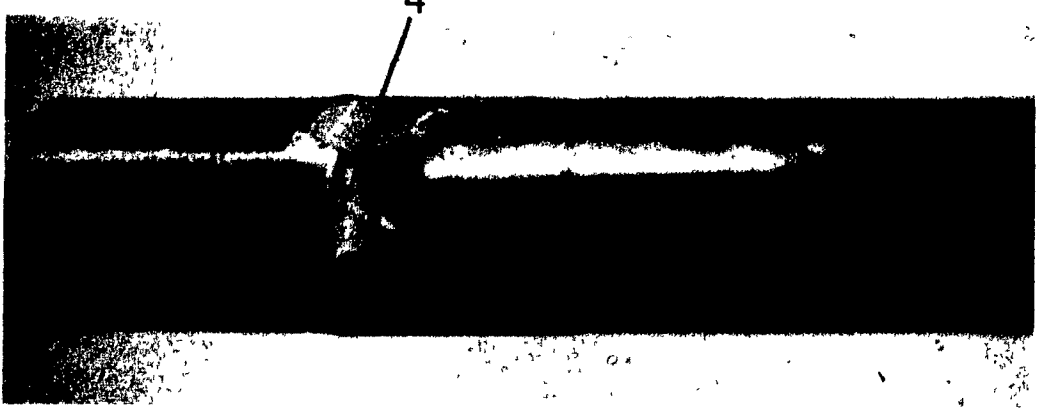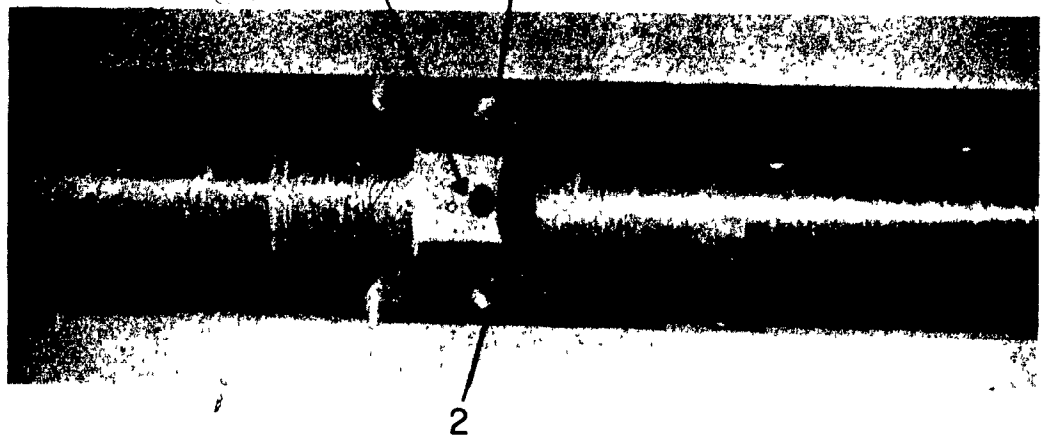
the surface pressure distribution around the probe. If the probe

is placed in a flow field such that the total mean velocity vector

is at some angle to the axis of the center tapping, then a pressure

differential will be set up across these holes, the magnitude of

which will depend upon the geometry of the tappings' positions on

the probe, and the magnitude and direction of the velocity vector.

Each probe requires calibration of the pressure differentials

between holes as a function of yaw and pitch angle. For Mach num-

bers less than 0.2, calibration is independent of Mach number,

Reynolds number and turbulence intensity up to 30%. It is pre-

ferable to rotate the probe until the yaw pressures are equal,

measure the angle of probe rotation (yaw angle) and determine the

pitch angle from the remaining pressure differentials. The use of

a pressure transducer for measurement of pressure differentials is

recommended, particularly for differential pressures of the order

of 0.10-mm water gauge or less.

If the probe is rotated to give $P_2 = P_3$ (see Figures 3 and

4), the yaw angle is read from an orientation gear and

$$\theta = C (P_4 - P_5) / (P_1 - P_2) \tag{3}$$

$$(P_T - P_S) / (P_1 - P_2) = K(\theta) \tag{4}$$

$$(P_1 - P_T) / (P_T - P_S) = F(\theta) \tag{5}$$

The equations permit the calculations of the velocity components.

The curves for $C(\theta)$, $K(\theta)$, and $F(\theta)$ are obtained from calibration.

Bryer and Pankhurst (30) show that calibration charts obtained for

a probe comprising five tubes of outside diameter 1.2-mm and inside diameter 0.9-mm were essentially the same at wind speeds of 18 m/s and 27 m/s.

When $P_T - P_S$ is found from the above equations it gives us the vector velocity intensity through equation:

$$P_T - P_S = C_p \; 1/2\rho V^2 \tag{6}$$

where
$$C_p = f(VD/\nu) = f(Re)_D \tag{7}$$

The value of C_p is very near unity. It was stated (31) that a Reynolds number of 30, where the characteristic size is the measuring tap diameter, is the minimum necessary to avoid viscous effects. At lower Reynolds numbers, the indicated pressure becomes higher than the actual stream impact pressure due to viscosity effects. This is also the conclusion drawn by Chue (32). This condition is attained in air for velocities under 3.5 m/s with impact holes of 0.25-mm.

Bryer and Pankhurst (30) stated that the lower limit of the Reynolds number (based on the external diameter), where viscous effects begin to be significant, can be a serious disadvantage for a small probe at low wind speeds. For example, a spherical probe would not be suitable for a range of wind speeds extending below 5 m/s unless the sphere is of at least 6-mm diameter.

From the above considerations, one would always choose a probe that is large enough to avoid viscous effects. However, it

should not be too big to cause interferences with the flow. Reference (33) shows that for a probe's cross sectional area smaller or equal to 1% of the cross sectional area of the stream, these secondary errors are negligible.

Although the effect of turbulence on the performance of five-channel probes has not been extensively investigated, there is some evidence (30) that where the size of the probe is small compared to the scale of turbulence, the centre tube gives at least as high a time-average value of total pressure as a plain pitot tube of the same inside-to-outside diameter ratio as that of the individual tubes of the five-tube probe. It was also found that static pressures can be obtained with an accuracy similar to that given by most other probes. Measurements made in the fluctuating wake flow behind a flat plate held normal to the stream have shown fair agreement between the measurements of velocity with a five-tube probe and with a hot-wire probe.

The variation of C_p with Reynolds number (see Equations 6 and 7) that may be caused by changes of turbulence in the stream is a secondary effect of turbulence. A more direct effect (32, 34) is due to the pressure changes at the total-head and static orifices produced by the turbulent velocity fluctuations that practically always occur. The flow may be regarded as having a steady velocity on which is superimposed a random turbulent velocity which has an average value of zero taken over a sufficiently long time interval. The fluctuating components of the velocities are v_x, v_y, v_z parallel

to the axes of a three-dimensional system of cartesian coordinates

with the x-axis along the direction of the mean flow. At any

instant, the velocity component in the x-direction is $V + v_x$; v_x

may be positive or negative, but its average value is zero and

similarly for v_y and v_z. The associated pressure changes, however,

depend on the squares of the velocities, and the mean value of these

is _not_ zero and, consequently, the turbulent velocity components

affect the readings of the pitot and static tubes. These effects

were investigated theoretically by Goldstein (35), neglecting pos-

sible effects of such factors as frequency, damping, resonance, and

lag in the leads. Subject to these limitations, it was shown that

the pressure measured by the pitot tube in incompressible flow is

not $P_S + \rho V^2/2$ but $P_S + \rho[V^2 + \overline{v_x^2} + \overline{v_y^2} + \overline{v_z^2})]/2$, where $\overline{v_x^2}$, $\overline{v_y^2}$, $\overline{v_z^2}$

are the mean squares of the turbulent components v_x, v_y, v_z. Gold-

stein's analysis showed also that the static tube might be expected

to record a pressure equal to $P_S + \rho[(1/2)(\overline{v_y^2} + \overline{v_z^2})]/2$. In iso-

tropic turbulence the reading of the pitot-static _combination_ will

be $\rho V^2(1 + 2\overline{v_x^2}/V^2)/2$.

The above results have been used extensively. But tur-

bulence can also be regarded as a statistical assembly of a vast

number of eddies of various sizes and Barat (36) pointed out that

its effects depend not only on the turbulence intensity measured by

$\overline{v_x^2}$, etc., but also on the Eulerian scale of turbulence. When the

size of a typical eddy is small compared to the diameter of a

static-pressure tube, the pressure fluctuations at the several

orifices will not be correlated. The opposite would happen with large eddies, as if the flow direction at any instant were inclined to the tube. The tube would then be expected to read low, by an amount corresponding to some sort of time average of the fluctuating angle of yaw or angle of pitch (31) in the case of a three-dimensional sensor.

It was shown that the error in the limit of indefinitely large scale turbulence is equal in magnitude and opposite in sign to the limit for indefinitely small scale, although no information is available about how the errors vary between the two limits which were found to be $\pm\rho(\overline{v_y^2} + \overline{v_z^2})/2$.

Presently, it is suggested that a pitot-static combination in isotropic turbulent flow will record (34) $\rho V^2(1 + \alpha\, \overline{v_x^2}/\overline{V^2})/2$, where $1<\alpha<5$ and the lower and higher limits correspond to infinitely small scale and infinitely large scale, respectively. Thus even if the R.M.S. turbulent velocity fluctuations are as great as 10 per cent of V, the error in velocity measurement, if the turbulence effects are neglected, amounts only to 0.5 - 2.5 per cent. As a value of $\sqrt{v_x^2}/V$ of 0.1 represents a fairly high intensity of turbulence, we may conclude that turbulence effects on pitot-static readings are often negligible.

It is known that the wedge shape probes cause less interference to the flow (30) then most other types, besides being easier to introduce in the flow field through the ports. The effects of

the gradients of velocity, static pressure and total pressure can

be of some importance when the direction of the gradient is from

one sensing hole to another. The separation distance between the

holes should then be as small as possible. It is found in prac-

tice that errors in angle measurements due to gradients of total

pressure, with little variation in static pressure, depend on the

type of probe being used and that, for a given separation of sensing

holes, the wedge-types are least subject to error. When comparing

wedge and traverse cylinder probes which have the tappings drilled

on the cylindrical surface and no wedge form is incorporated,

errors from total-pressure gradient effects are found (37) to be

much larger for the transverse-cylinder probe than for the wedge

probe, having similarly spaced sensing holes and recording pres-

sures close to the free-stream static. Due to the geometric

similarity between the wedge-type probes and the cylinder-type

shown in Figure 4, one may conclude that they present similar

characteristics.

Flow Sense Indicator

Sometimes it is necessary to determine the general direc-

tion of the velocity vector in the vortex flow before introducing a

measuring instrument into it. For example, introducing a 5-channel

pressure probe pointing in the direction opposite to the main flow

will result in erroneous measurements, although the indications of

yaw tappings' pressure are that the probe is aligned with the flow

direction. Chigier (16) recommends that the direction of the flow

be first ascertained by means of tuft grids or of a simple flow
sense indicator consisting of a tube with two pressure taps in the
side walls facing opposite directions. This probe is also claimed
to be useful for the determination of reverse flow boundaries.

Static Pressure Sensors

Static pressure gradients occur in all vortex flows as a
consequence of tangential velocity gradients and of the associated
centrifugal forces, as well as of variations in turbulence intensity.
Care must be taken (15) in the measurement of static pressure in
turbulent vortex flows in order to avoid contributions from the
dynamic pressure. The static pressure measuring surface must be
aligned with the local velocity vector. Miller and Commings (38)
used a disc static probe in their study of single and dual air jets,
and the reliability of the results obtained was good when they
balanced pressure and shear terms in the equation of motion.
Chigier and Beer (39) modified this probe for use in swirling flows,
by fitting a simple yaw meter - two hypodermic tubes with edges
sawn off at 45° - fitted to the underside of the disc with the tubes'
axes parallel to the disc's surface. The disc is rotated until the
pressure differential in the yaw tube is zero and then the static
pressure is measured via the static-pressure tapping. This was the
only type of specifically static-pressure measuring devices reported
to have success in vortex flows found in the literature.

The most common example of static-pressure probe consists

of a body of revolution with its axis aligned with the flow. The
measuring orifice is located at a position where the pressures on
the surface aligned with the flow are equal. This only happens a
few stem diameters downstream from the tip. In order to reduce
errors due to misalignment with the flow, it is usual to provide
several orifices around the probe which intercommunicate inside the
instrument, so that the mean pressure is recorded (30). In sub-
sonic flows, the effect of the stem of the instrument is to increase
the upstream static pressure above that of the free stream, and so
the pressure field of the stem can be used to balance locally the
pressure fall caused by the nose. A pressure tapping located in
the region where the head effect and the stem effect balance can
therefore record the free-stream static pressure accurately. In
practice, if the balance is not exact, the error will be known from
calibration. In order to have good accuracy in vortex flows, the
type of probe should consist of a stem with the same curvature as
the vortex flow at the measuring point or, alternatively, the length
of the stem should be negligible relative to this curvature. This
is due to the requirement that the probe axis should always be
parallel to the mean velocity vector to avoid secondary dynamic
pressure effects.

It has already been mentioned that five-channel pressure
probes can measure static pressures as accurately as most other
static pressure probes. These static pressures can be easily
calculated from Equations (3), (4), and (5) and the value of

$(P_\lambda - p_{atm})$.

SUMMARY

It can be concluded from this part of the review that the simplicity, good resolution and accuracy of five-channel pressure probes makes them most appropriate for vortex flows' velocity measurements. For static pressure measurements, these instruments show an accuracy similar to that of other static-pressure probes (30) and have the great advantage of permitting the simultaneous measurement of this pressure along with the velocity components. However, they are not well suited for measurements at very low velocities or in close vicinity to a solid surface.

Hot-wire anemometers are also well suited for mean velocity measurements, as well as their fluctuating components, although they are more delicate and require electronic circuitries. They are the most probable choice if turbulence or transient responses are required. They are capable of measuring lower velocities than the five-channel pressure probes. Obviously, no static-pressures can be measured.

It was noted that turbulence effects are likely to be small on the pressure instrument (34, 35, 36) although care has to be taken in very turbulent cases. Viscous effects can also be neglected if the probe is chosen carefully (30, 31, 32, 33). When these effects are unavoidable, correction is possible (32). A

compromise for the size of the probe has to be found: its cross-sectional area should not be larger than 1% of that of the flow (33) so that interferences in the flow pattern become negligible, and it should be large enough to have a $Re_d > 30$ to avoid viscous effects (31, 32). The distance between the sensing holes should be as small as possible in order to avoid velocity and pressure gradient effects. For this, the wedge-cylinder type seems the most suitable (37).

NOMENCLATURE

NOMENCLATURE

C	–	Five-channel probe calibration factor
C_p	–	Pressure-probe calibration factor
D	–	Outside diameter of pressure probe
f	–	Function
F	–	Five-channel probe calibration factor
k	–	Koval and Mikhailov's tangential velocity profile parameter
k_1, k_2	–	Constants
K	–	Five-channel probe calibration factor
P_1	–	Probe's centre tapping pressure (see Figure 4)
P_2, P_3, P_4, P_5	–	Probe's side tappings' pressures (see Figure 4)
P_{atm}	–	Atmospheric pressure
P_S	–	Static pressure
P_T	–	Total pressure
r	–	Radius
R	–	Radius of chamber
$(Re)_D$	–	Reynolds number where characteristic size is probe's external diameter
$(Re)_d$	–	Reynolds number where characteristic size is probe's tap diameter
$(Re)_r$	–	Reynolds number based on radial position in chamber and radial velocity
u	–	Radial velocity

u_o —   Radial velocity at the outer radius of chamber

V —   Velocity

v_x, v_y, v_z —   Turbulent velocity fluctuations in cartesian coordinates

w —   Tangential velocity

w_R —   Tangential velocity at radius R

Greek Letters

α —   Turbulence scale coefficient

ε —   Eddy (kinematic) viscosity

λ —   Rietema and Krajenbrink's tangential velocity profile parameter (Equation 1)

ν —   Fluid kinematic viscosity

ρ —   Fluid density

θ —   Pitch angle

BIBLIOGRAPHY

BIBLIOGRAPHY FOR LITERATURE REVIEW

1. Marshall, W.R., Jr., 'Atomization and Spray Drying', _Chem. Eng. Progress Monograph Series_, Vol. 50, No. 2, (1954)

2. Katta, S., and Gauvin, W.H., 'Some Fundamental Aspects of Spray Drying', _A.I.Ch.E. Journal_, Vol. 21, No. 1, (1975), 143

3. Perry, J.H., 'Chemical Engineers' Handbook', McGraw-Hill Book Co., 4th Edition

4. Koval, V.P., and Mikhailov, S.L., 'Velocity and Pressure Distribution of Liquid in a Swirl Chamber', _Teploenergetika_, Vol. 19, No. 2, (1972), 25-28

5. Syred, N., and Beer, J.M., 'Combustion in Swirling Flows: A Review', Combustion and Flame, Vol. 23, (1974), 143-201

6. Mensing, A.E. et al., 'Investigation of the Use of a Vortex Flow to Separate Oil from an Oil-Water Mixture', _United Aircraft Research Laboratories_, Report 714/03/A/001, (Nov. 1970)

7. Baddour, R.F., and Timmins, R.S., 'The Application of Plasmas to Chemical Processing', _MIT Press_, 1967

8. Gardeman, D.A., and Hecht, N.L., 'Arc Plasma Technology in Material Science', _Springer-Verlag_, 1972

9. Pfender, E., 'Generation of an Almost Fully Ionized, Spectrally Clean, High Density Hydrogen Plasma', _Proceedings of the 6th International Conference on Ionization Phenomena in Gases_, Edited by P. Hubert and E. Crémieu-Alcan (Paris, 1963), Vol. II, pp.369-374

10. Hilsch, R., 'The Use of Expansion of Gases in a Centrifugal Field as a Cooling Process', _Review of Scientific Instruments_, Vol. 18, No. 2, (Feb. 1947), 108

11. Baluev, E.D., Troyankin, Yu. V., 'The Effect of the Design Parameters on the Aerodynamics of Cyclone Chambers', _Teploenergetika_, Vol. 14, No. 2, (1967), 67-71.

12. Baluev, E.D., Troyankin, Yu. V., 'Study of the Aerodynamic Structure of Gas Flow in a Cyclone Chamber', _Teploenergetika_, Vol. 14, No. 1, (1967), 63-65

13. Bank, N., and Gauvin, W.H., 'Measurements of Flow Characteristics in a Confined Vortex Flow', _The Canadian Journal of Chemical Engineering_, Vol. 55, (1977), 397

14. Bank, N., and Gauvin, W.H., 'Inclined Hot-Wire Response Equations for a Flow Field Having a Dominant Tangential Velocity Component', The Canadian Journal of Chemical Engineering, Vol. 55, (1977), 516

15. Bank, N., 'Measurements of Flow Characteristics in a Confined Vortex Flow', M. Eng. Thesis, Department of Chemical Engineering, McGill University, (1975)

16. Chigier, A.N., 'Velocity Measurement in Vortex Flows', A.S.M.E. Paper No. 5-1-31, (May 1971)

17. Rietema, K., and Krajenbrink, H.J., 'Theoretical Derivation of Tangential Velocity Profiles in a Flat Vortex Chamber - Influence of Turbulence and Wall Friction', Appl. Sci. Res., Vol. 8, Section A, (1958)

18. Schowalter, W.R., and Johnstone, H.F., 'Characteristics of the Mean Flow Patterns and Structure of Turbulence in Spiral Gas Streams', A.I.Ch.E. Journal, Vol. 6, No. 4, (1960), 649

19. Kendall, J.M., Jr., 'Experimental Study of a Compressible Viscous Vortex', J.P.L. Rep. TR32-290, (1962)

20. Kotas, T.J., 'Turbulent Boundary Layer Flow on the End Wall of a Cylindrical Vortex Chamber', Heat and Fluid Flow, Vol. 5, No. 2, (1975), 77

21. Troyankin, Yu. V., and Baluev, E.D., 'The Aerodynamic Resistance and Efficiency of a Cyclone Chamber', Teploenergetika, Vol. 16, No. 6, (1969), 29

22. Ogawa, A., 'On the Pressure Drop of Cyclone-Dust-Collectors', J. Coll. Engng. Nihon Univ., Series A, 16, (1975), 33

23. Ogawa, A., 'On the Flow Pattern of the Turbulent Rotational Flow in the Returned Type of the Vortex Chamber', J. Coll. Engng. Nihon Univ., Series A, 17, (1976), 51

24. Ogawa, A., 'On the Stability Criterion of the Fine Solid Particles in the Turbulent Rotational Flow', J. Coll. Engng. Nihon Univ., Series A., 18, (1977), 87

25. Arya, S.P.S., and Plate, E.J., 'Hot-Wire Measurements in a Thermally Stratified Flow', Research Memorandum No. 11, Fluid Dynamics and Diffusion Laboratory, College of Engineering, Colorado State University, Fort Collins, Colorado

26. Chevray, R., and Tutu, N.K., 'On Velocity Measurements in Non-Isothermal Turbulent Flows', Report No. 211, State University of New York at Stony Brook, August 1971

27. Corrsin, S., 'Turbulence: Experimental Methods', Reprint From Encyclopedia of Physics, Edited by S. Flügge/Freiburg, Volume VIII/2 Springer-Verlag/Berlin-Gottingen-Heidelberg 1963

28. Gessner, F.B., and Moller, G.L., 'Response Behaviour of Hot Wires in Shear Flow', J. Fluid Mech., Vol. 47, Part 3 (1971), 449

29. Bryer, D.W., Walshe, D.E., and Garner, M.A., 'Pressure Probes Selected for Three-Dimensional Flow Measurement', Reports and Memoranda No. 3037, National Physical Laboratory, November 1955

30. Bryer, D.W., and Pankhurst, R.C., 'Pressure-Probe Methods for Determining Wind Speed and Flow Direction', N.P.L. - London: Her Majesty's Stationery Office, (1971)

31. United Sensor & Control Corp., 'Pitot-Static Pressure Probes', Bulletin 1

32. Chue, S.H., 'Presure Probes for Fluid Measurement', Prog. Aerospace Sci., Vol. 16, No. 2, (1975), 147

33. United Sensor & Control Corp., 'Theory and Application of Fluid Flow Probes', Technical Bulletin T-2

34. Ower, E., and Pankhurst, R.C., 'The Measurement of Air Flow', Pergamon Press, 7th Edition, (1966)

35. Goldstein, S., 'A Note on the Measurement of Total Head and Static Pressure in a Turbulent Stream', Proc. Roy. Soc. A 155, (1936), 570

36. Barat, M., 'Influence de la Turbulence sur les Prises de Pression Statique', Comptes Rendus 246, (1958), 1156

37. Gagliardi, F.A., Cederberg, G.A., 'The Effect of Hole Geometry and Angle of Attack Variation on the Total Pressure Recovery of Cylindrical Pressure Probes', Westinghouse Electric Corporation, Aviation Gas Turbine Division, Engineering Department, Report No. A-1413, (1951)

38. Miller, R.D., and Comings, E.W., J. Fluid Mech., Vol. 7, No. 2, (1960), 237-256

39. Chigier, N.A., and Beer, J.M., Journal of Basic Eng. Trans. A.S.M.E., Series D, Vol. 86, No. 4, (1964), 788-796

40. Gyarmathy, G., 'Optical Measurements of Mass Density in a High-Speed, Confined, Gaseous Vortex', AIAA J., Vol. 7, 10 (1969), 1838

EXPERIMENTAL SECTION

INTRODUCTION

For the past many years this laboratory has been engaged in the study of the fundamental principles of the spray-drying process, only a few of which will be mentioned here (1, 2, 3). These investigations have demonstrated the importance of droplet trajectories, since they completely govern the transport phenomena involved in the drying process. These trajectories, in turn, are entirely dependent on the patterns of the entraining gas in vortex motion and the magnitude of the three components of its mean-flow velocity. This is only one of the many examples of the importance of a sound knowledge of vortex motion for the proper design and operation of industrial equipment in which use is made of this type of motion. Others are cyclone dust separators, gas scrubbers, absorbers, spray coolers (4), oil-water separators (5), centrifugal burners (6, 7), and, recently, plasma flame stabilization (8, 9, 10). In its major field of applications, namely, heterogeneous systems in which dispersed droplets or small particles are contacted with the entraining gas, use is made of the aptitude of the swirl to promote dispersion and mixing, to separate substances of different specific gravity or physical characteristics, and to lengthen the contacting time between the two phases.

The prediction of the three-dimensional velocity profiles as function of the operating conditions and geometry of the vortex

system is probably the most important aspect for its proper design
and operation. The complexity introduced by the three-dimensional
character of the motion and the existence of secondary flows in the
confining equipment have so far hindered the complete understanding
of the detailed mechanics of vortex flow. Many investigations have
oversimplified the complexities of the flow and only a few analyses
have considered the effect of geometrical parameters (11, 12, 13).

From a review of the published literature, experimental and
theoretical results of most workers agree in the following important
properties of the confined vortex flows, most of which were noted by
Bank and Gauvin (3, 14):

i.   The confined vortex flow pattern is three-dimensional
in nature (3, 6, 12, 13, 14, 15, 18).

ii.   The tangential velocity component is predominant and
the radial velocity component is very small in the entire vortex
flow (3, 12, 14, 15, 16, 18, 20).

iii. An important downward axial flow occurs in an annular
region adjacent to the wall (3, 12, 13, 14, 15). Some workers also
measured a substantial axial flow in the maximum tangential velocity
component region (12, 13).

iv.   The axial velocity may show a reversal near the axis
of the vortex chamber (3, 12, 13, 14).

v.   The tangential velocity profile in the radial direction
is composed mainly of two regions: a peripheral region of quasi-free

vortex (where $wr = k_1$ is approximated) and a central part of
quasi-forced vortex flow (where $w = k_2 r$ is approximated) (12, 13,
16, 17, 19).

vi.   In a vortex flow, there may be a helical-shaped
dynamic axis of symmetry (3, 14, 20).

vii.   It seems that the angle of inlet flow may change the
axial flow pattern, mainly near the walls of the vortex chamber (3,
7, 14).

viii. The static pressure is high near the vortex flow
confining walls and decreases drastically near the axis, where it
reaches its minimum (7, 15, 19).

The present study is a continuation of Nader Bank's work
in this laboratory (3, 21, 14). Briefly summarized, Bank's measure-
ment technique was based on the use of a single hot-wire anemometer
probe, rotated in eight different azimuthal directions at a given
position in the flow. Appropriate response equations for this
special condition first had to be derived theoretically (21). He
then measured the velocity profiles of the ambient temperature air
vortex flow generated in a chamber with a cylindrical top containing
six small symmetrically distributed inlet ports, and a conical
bottom (3). His experiments were limited to low volumetric flow
rates and his inlet velocity did not exceed 3.2 m/s. Because the
velocities were so small, his experimental technique prevented him
from measuring any radial velocities, as well as the axial velocities
at any except the higher velocities. On the other hand, he was able

to provide one of the first reported measurements of radial dis-
tributions of tangential and axial intensities of turbulence for
swirl systems. He did not attempt to make any static pressure
measurements.

Nader Bank's chamber was modified for the present investi-
gation to provide visualization inside the equipment and the control
of the inlet flow angle, a parameter identified as of possible
importance by Bank and also by Syred (7). Most importantly, the
range of volumetric flow rates was increased considerably.

A five-channel pressure probe was used in the present work
to improve resolution and simplicity in the measurement of the mean
velocity components and, additionally, to obtain static pressure
profiles throughout the vortex chamber.

The objectives of this study were, more specifically, to
investigate the effects of the inlet gas flow rate and of the angle
of inlet flow on the static pressure and velocity fields, as a
function of the position in the chamber. The experimental program
was preceded by the theoretical derivation of a correlation for the
tangential velocity from first principles as a function of the flow
parameters, to permit the subsequent comparison of this prediction
with the experimentally-observed values.

THEORETICAL DERIVATION

Some theoretical studies on the equations for the tangential

velocity profiles have been published in the literature. In

general, they agree on the existence of a central forced-vortex

region while the main part of the flow approximates a free-vortex

pattern. Most of these authors attempted to derive equations for

the velocity and static pressure profiles, the most important of

which is the tangential velocity profile. The experimental data

obtained on the patterns of flow of liquids and gases in swirl

chambers of different types permitted the adoption of initial

assumptions in the theoretical derivations. One important

assumption concerns the applicability of the Navier-Stokes equation

of motion to describe the flow, replacing the kinematic viscosity

$\underline{\nu}$ by the total kinematic viscosity $\underline{f}$ (6, 17). The value of $\underline{f}$ is

$\nu + \varepsilon$, where $\underline{\varepsilon}$ is the turbulent kinematic viscosity. In practice,

the kinematic fluid viscosity can be neglected with respect to the

turbulent kinematic viscosity. The turbulent kinematic viscosity

coefficient is dependent on the scale of turbulence and on the

Reynolds number given by Equation (10) of this section.

This section will concentrate on the development of a

theoretical equation of a general form for the main part of flow

(quasi-free-vortex) with the least possible restricting assumptions

in the governing equations. A conical geometry can be assumed for

all derivations. This will be followed by derivation for a theo-

retical forced-vortex tangential velocity profile.

For the free-vortex region of the flow, the Navier-Stokes

and continuity equations, replacing the kinematic coefficient of

viscosity by the total kinematic viscosity, are:

$$u(\delta u/\delta r) - (w^2/r) = -(1/\rho)\ (\delta p/\delta r) +$$
$$f[(\delta^2 u/\delta r^2) + (1/r)\ (\delta u/\delta r) - (u/r^2)] \qquad\qquad (1)$$

$$u(\delta w/\delta r) + (uw/r) = f[(\delta^2 w/\delta r^2) + (1/r)\ (\delta w/\delta r) -$$
$$(w/r^2)] \qquad\qquad (2)$$

$$u(\delta v/\delta r) = -(1/\rho)\ (\delta p/\delta z) +$$
$$f\{(1/r)\ \delta/\delta r\ [r(\delta v/\delta r)]\} \qquad\qquad (3)$$

$$\delta(ru)/\delta r = 0 \qquad\qquad (4)$$

The assumptions in the above equations were:

a. No time dependence, i.e., steady state is reached.

b. Body forces are unimportant.

c. The variation of the physical quantities in the angular direction is zero, or, the flow is axisymmetric. That is: $\delta u/\delta\theta \cong \delta w/\delta\theta \cong \delta v/\delta\theta \cong \delta p/\delta\theta \cong 0$. It is known that in some cases the axisymmetry is not attained in real vortices (14).

d. The vertical (axial) gradients of circumferential, axial and radial velocities are much smaller than these gradients in the radial direction. This assumption was supported by results of measurements made by Ogawa (15).

e. Density (ρ) and turbulent total viscosity (f) are constant.

Integrating equation (4), one obtains:

$$u = C_1/r \qquad\qquad (5)$$

Making a mass balance through a cylindrical surface of

radius $\underline{r}$, where $r > R_0$ (radius of chamber's outlet) for the free-vortex region, and a height $\underline{h}$ measured from the top of the chamber, to the intersection of $\underline{r}$ with the wall of the chamber, one obtains:

$$W = -2\pi r u h \rho \qquad (6)$$

$$u = -W/2\pi r h \rho \qquad (7)$$

where $\underline{W}$ = total mass flow rate entering the chamber. A constant radial velocity was assumed for all axial positions (this is assumption 'd' above).

Equation (2) can be rearranged as follows·

$$(u/r) \, \delta/\delta r(rw) = f\{\delta/\delta r \, [(1/r) \, \delta/\delta r \, (rw)]\} \qquad (8)$$

Integrating this last equation, the angular momentum relative to the chamber's axis is obtained:

$$rw = C_2 \int r \exp \left[\int (u/f) \, dr\right] dr + C_3 \qquad (9)$$

Substituting (7) in (9):

$$\int (u/f) \, dr = -k \, \ln r \qquad (10)$$

where $\quad k = W/2\pi h f \rho \qquad (11)$

The physical significance of either side of Equation (10) is that they represent the Reynolds number for the velocity and radius considered.

Substituting (10) in (9):

$$rw = C_2 \int r \exp[-k \ln r]\, dr + C_3$$

or $$rw = C_2 \int r^{1-k}\, dr + C_3 \qquad (12)$$

A) For $k \neq 2$:

$$rw = C_2\, r^{2-k}/(2-k) + C_3$$

or $$rw = C_4\, r^{2-k} + C_3 \qquad (13)$$

where $C_4 = C_2/(2-k)$

The boundary conditions for an axisymmetric vortex are:

i. When $r \to 0$, $wr \to 0$ and so, $C_3 = 0$

• In other words, as the axis of the chamber is approached, the momentum <u>wr</u> approaches zero.

ii. When $r \to R$, $wr \to w_R R$ and so, $C_4 = w_R/R^{1-k}$

In other words, as the wall of the chamber is approached, the momentum approaches $w_R R$ where w_R is the tangential velocity at radius <u>R</u> and <u>R</u> is the internal radius of the chamber.

Substituting for C_3 and C_4:

$$w = w_R (r/R)^{1-k} \qquad (14)$$

B) For $k = 2$ in Equation (12):

$$rw = C_2 \int (1/r)\, dr + C_3$$

or $$rw = C_2 \ln r + C_3$$

Accounting for the same boundary conditions as before, one obtains:

i.   When $r \to 0$, $rw \to 0$ and so, $C_2 = 0$

ii. When $r \to R$, $rw \to Rw_R$ and so, $C_3 = Rw_R$

Substituting for C_2 and C_3 in this case, one obtains:

$$w = w_R \ (R/r) \tag{15}$$

Equations (14) and (15) predict theoretically the behaviour
of the tangential velocities for the free-vortex region at any axial
position as a function of the chamber's height, the flow rate passing
through the chamber and the total viscosity. This last parameter is
very difficult to obtain beforehand for the purpose of predicting
these velocity profiles.

For the central forced-vortex region, the derivation is as
follows:

From the vorticity equation (22) and assuming that constant
angular velocity exists in the forced-vortex region, one obtains:

$$\Omega_z = 2\omega_z = (w/r) + (\delta w/\delta r) -$$
$$(1/r) \ (\delta u/\delta\theta) = \text{constant} \tag{16}$$

Assuming that the variation of all physical quantities with
θ are equal to zero, this equation reduces to:

$$\Omega_z = (w/r) + (\delta w/\delta r) = \text{constant} \tag{17}$$

This equation can be written as:

$$(1/r) \ \delta/\delta r \ (wr) = A_1 \tag{18}$$

Integrating:

$$wr = A_1 \, (r^2/2) \tag{19}$$

or
$$w = Ar \tag{20}$$

The constant of integration was made zero from the condition $w = 0$ at $r = 0$. Equation (20) represents a fluid rotating like a solid body.

Together, Equations (14) and (20) represent theoretical approximations of the tangential velocity profiles for the entire radius of the chamber.

EXPERIMENTAL

APPARATUS

A schematic diagram of the experimental system is shown in Figure 1. A photograph of the vortex chamber used in the investigation is given in Figure 2, and its diagrammatical representation is illustrated in Figure 3. It had an overall height of 172 cm and consisted of a cylindrical and conical section. The upper cylindrical section was 61 cm in height and 61 cm in radius (internal sizes). It was constructed of 20-gauge galvanized steel with windows, top and tangential inlet made of plexiglass, a transparent material which permitted flow visualization. A single outlet of 7.48 in (19 cm) was located at the apex of the conical section. In order to study the effect of the outlet size an 11-cm high frustum

FIGURE 1

SCHEMATIC DIAGRAM OF EXPERIMENTAL SYSTEM

SIMPLIFIED DIAGRAM OF EQUIPMENT AND MEASURING SYSTEM

TANGENTIAL INLET WITH
FLOW ANGLE CONTROL

5-CHANNEL
PRESSURE-PROBE

VORTEX CHAMBER

ORIFICE
FLOWMETER

U-TUBE
MANOMETER

FLOW-CONTROL
VALVES

SCANNING
VALVE

THERMOMETER
BAROMETER

BLOWER

PRESSURE
TRANSDUCER

MANOMETERS

49
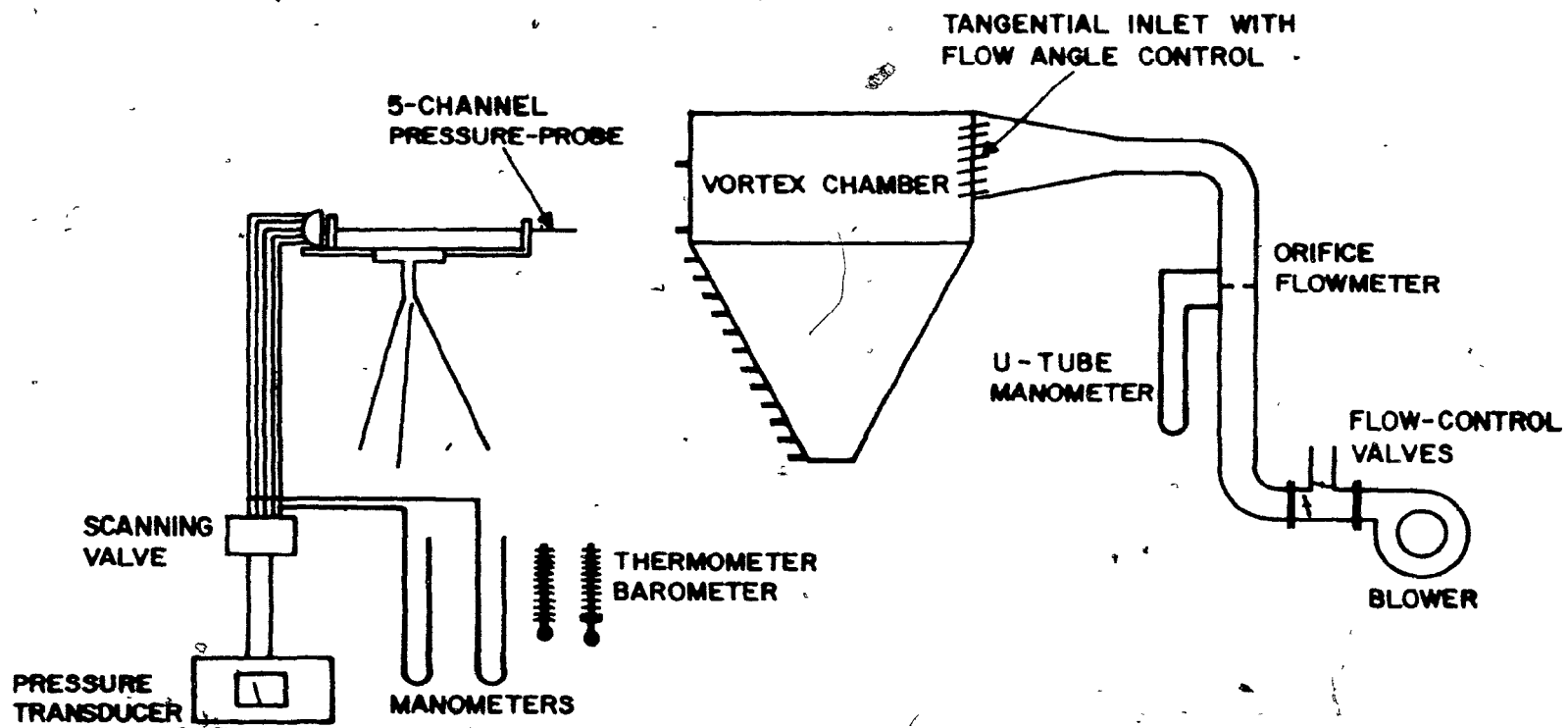
FIGURE 2

PHOTOGRAPH OF THE VORTEX CHAMBER
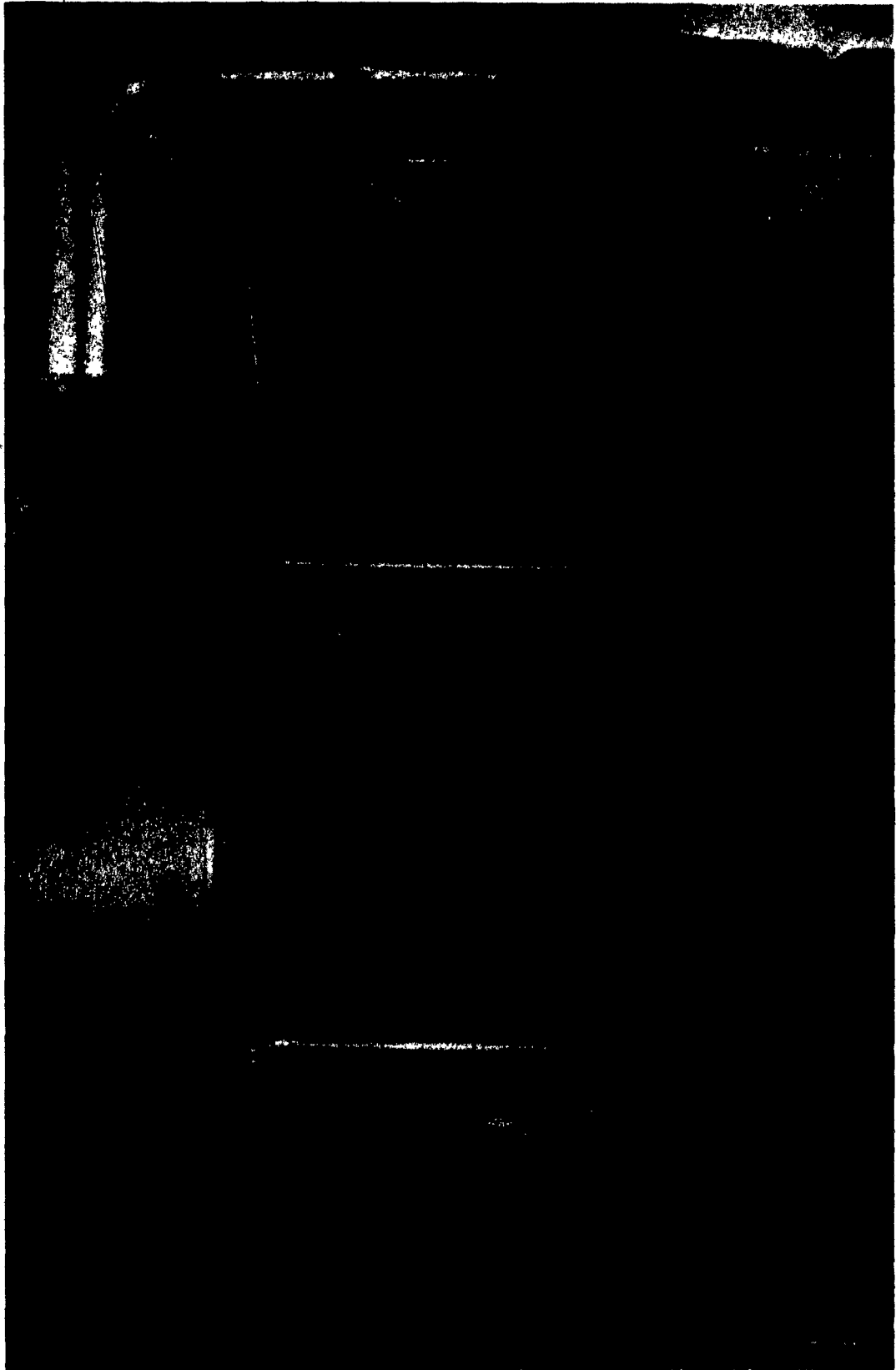
FIGURE 3

SCHEMATIC DIAGRAM OF THE VORTEX CHAMBER

SCHEMATIC DIAGRAM OF VORTEX CHAMBER

AIR FLOW

PLEXIGRASS WINDOWS

1219

610

250

200

1075

400

128

200

150

110

76

190

ALL SIZES IN mm
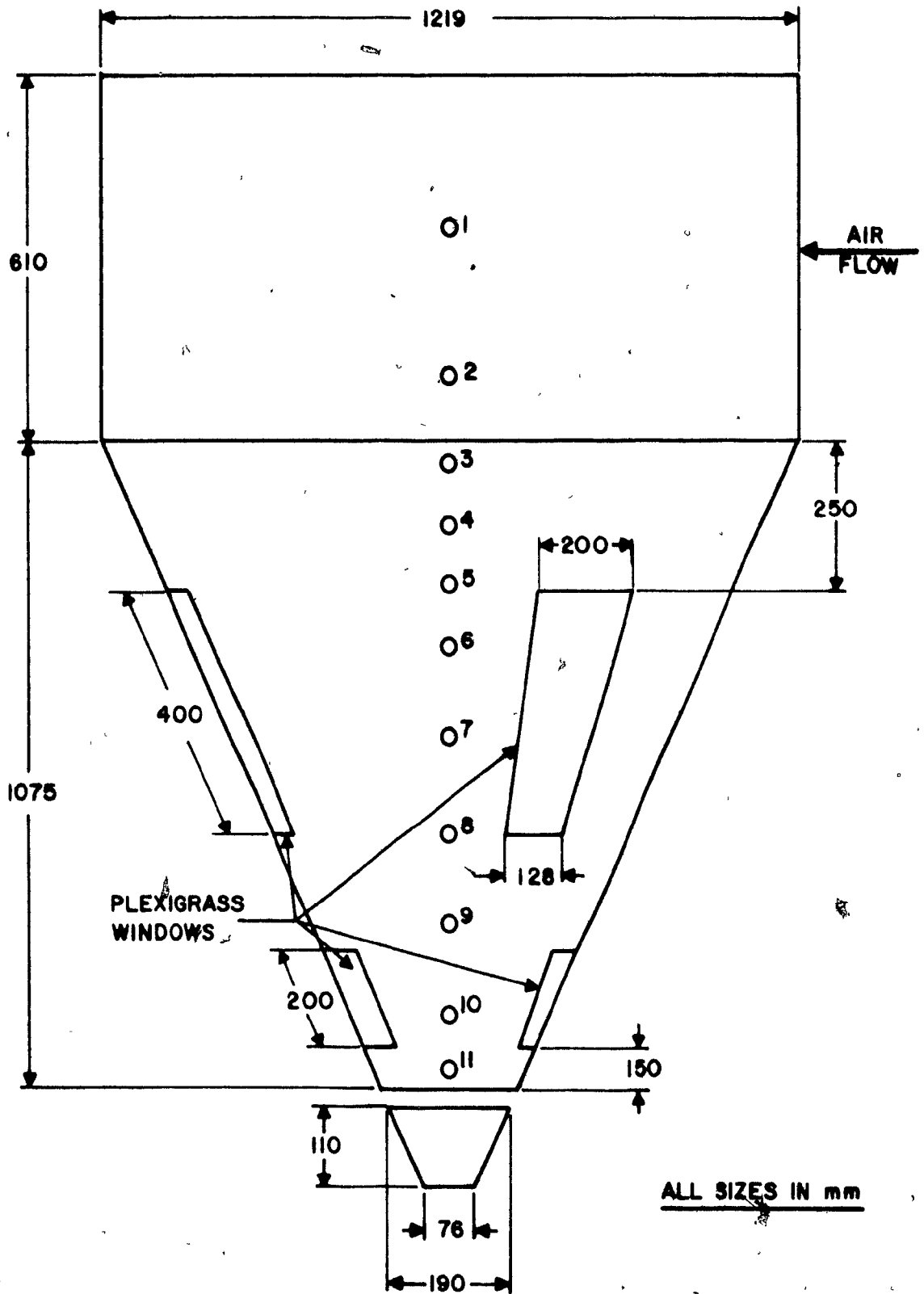
of a cone could be adapted to the outlet.

A motor-blower assembly, consisting of a 5-HP, 550-volt, 3-phase A.C. electric motor driving model Clarage-9G1 blower made by Canada Fans Limited and equipped with a type SS wheel, was used to provide different air flow rates to the chamber, with a maximum of 1300 CFM (0.61 m^3/s) at a static pressure of 7 in (17.8 cm) of H_2O. A 200-mesh stainless steel wire cloth filter with a total filtering area of 1550 cm^2 was adapted to the blower inlet. The outlet of the blower was connected to a three-way double-butterfly valve which controlled the flow. One of the valve's branches was connected to the tangential inlet of the chamber through a flexible connection to prevent the propagation of vibration to the test section.

The air flow rate was measured by a flowmeter consisting of a square-edged orifice of 2.78 in (7.06 cm) radius, installed in the outlet line of the blower, which had an inside diameter of 8 in (20.32 cm). The pressure differentials were measured between 'radius taps' located at the same line by means of a U-type manometer filled with 'meriam' liquid of density = 1.0 g/cm^3 (see Figure 10). The orifice flowmeter was calibrated by means of a standard 10-point traverse.

The atmospheric pressure was obtained from a barometer and was necessary to calculate the velocity pressures measured with the five-channel pressure probe. The inside temperature of the air in

the chamber was similarly recorded.

The air from the blower entered the cylindrical section tangentially at an angle which was contrólled by a system consisting of ten parallel aero-foil-shaped vanes linked to a common lever device. The sizes of the vanes were 12 cm x 10 cm and their maximum thickness was 0.6 cm. To the top and bottom vanes were attached plexiglass half-cylinders which turned together with these vanes. At any vane's angle, these cylindrical surfaces were pressed against a layer of synthetic felt attached to the top and bottom walls of the inlet, to ensure that no straight-flowing currents would perturbate the angle of flow.

The tangential inlet had a cylindrical cross section measuring 40 x 12 cm and is shown on Figure 4.

Along one vertical side of the chamber wall, eleven measuring ports were connected. These ports consisted of 7/16 in (1.11 cm) i.d. bushings with a 5/8 in (1.59 cm) thread to permit the installation of the probe's seal. Rubber corks were used to plug the ports when not in use. The locations of these ports are given in Table I. The distances shown are relative to the top of the chamber. Stations 1 and 2 were located on the cylindrical section and the others on the conical section.

At the position on the wall of the chamber diametrically opposite to port 6, another port, 6', was installed for the purpose of comparing results when traversing the five-channel probe from

FIGURE 4

PHOTOGRAPH OF THE TANGENTIAL INLET TO THE CHAMBER
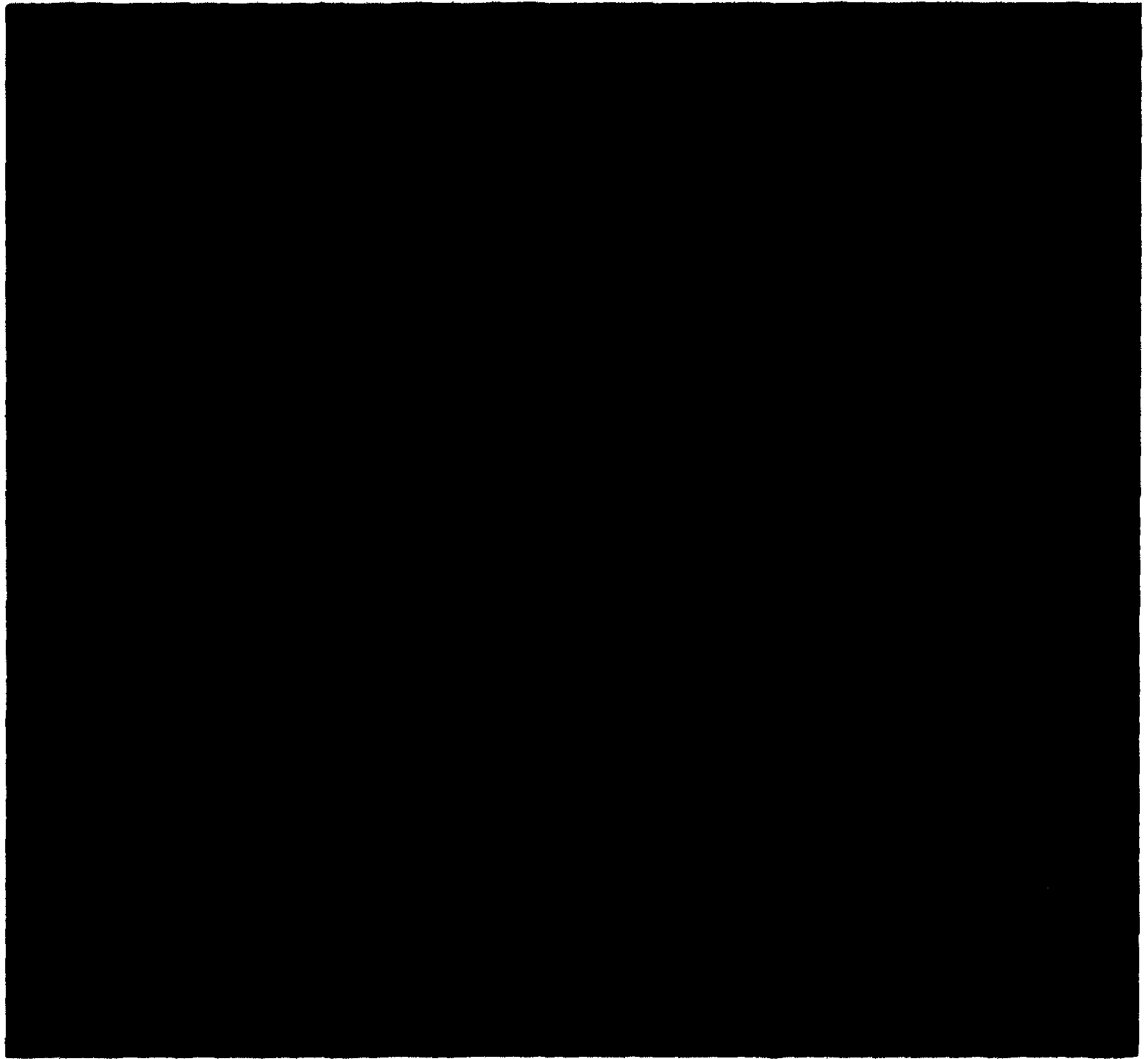
TABLE I

AXIAL AND RADIAL LOCATIONS OF THE MEASURING STATIONS

STATION NUMBER (See Figure 3)	AXIAL DISTANCE z-(cm)	CHAMBER RADIUS R-(cm)
1	25.1	61.6
2	50.2	61.6
3	64.2	59.8
4	74.3	55.1
5	84.5	50.3
6	94.6	45.5
6'	94.6	45.5
7	109.9	38.4
8	125.1	31.2
9	140.4	24.0
10	155.6	17.0
11	170.8	10.0

Equations for radius $\underline{R}$ of the conical section of the chamber, as a function of the axial position $\underline{z}$ are:

$$R = -.47z + 89.83 \text{ in cm}$$

$$\underline{o\ r}$$

$$R = -52.17 \frac{(z - zo)}{Z} + 61.26 \text{ in cm}$$

opposite sides.

Five plexiglass observation windows (three of 700 cm^2, and two of 460 cm^2) on the conical section, together with the entirely plexiglass-made top, provided good illumination and visibility for flow visualization.

INSTRUMENTATION

Five-Channel Pressure Probe

A close-up picture of the three-dimensional probe used for the measurement of the velocity and static pressure profiles in this work is shown on Figure 5.

The pressure probe was manufactured by United Sensor and Control Corporation with the specification DA-250-48-H-44-Cd. It was 6.4 mm in diameter up to a distance of 101.6 mm from the tip. At this position, the diameter increased to 7.9 mm to avoid vibrations. This reinforced part of the probe was 1117 mm in length. The tip extended two diameters beyond the measuring taps. The five holes were distributed symmetrically on the five planes provided on the cylinder as can be seen from Figure 5. A centrally-located hole measured P_1, the pressure which permits the

FIGURE 5

CLOSE-UP PICTURE OF FIVE-CHANNEL PRESSURE PROBE
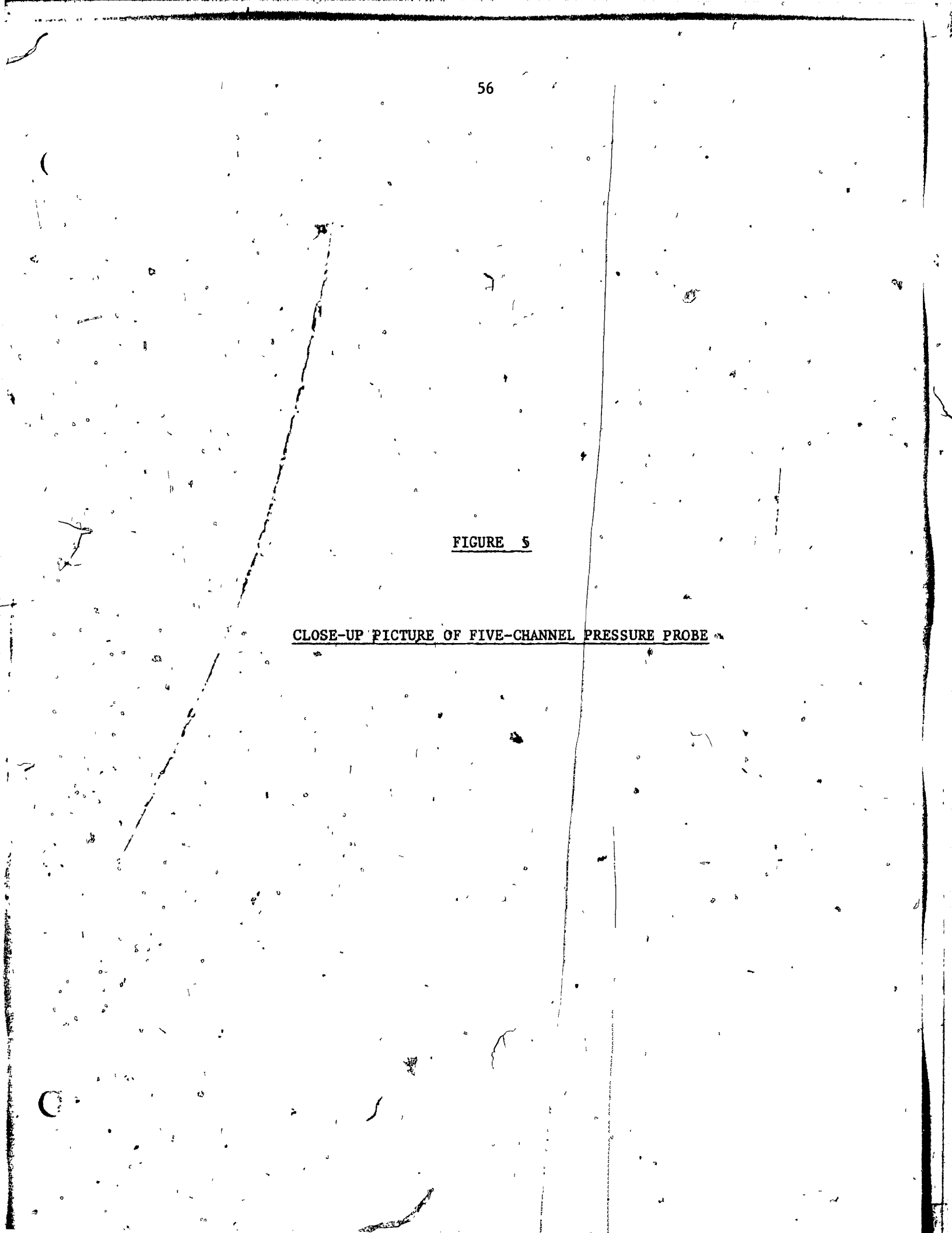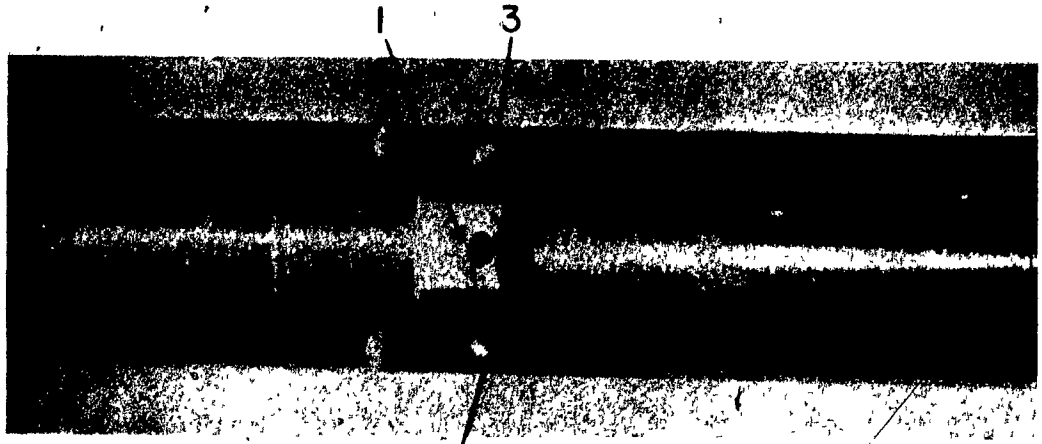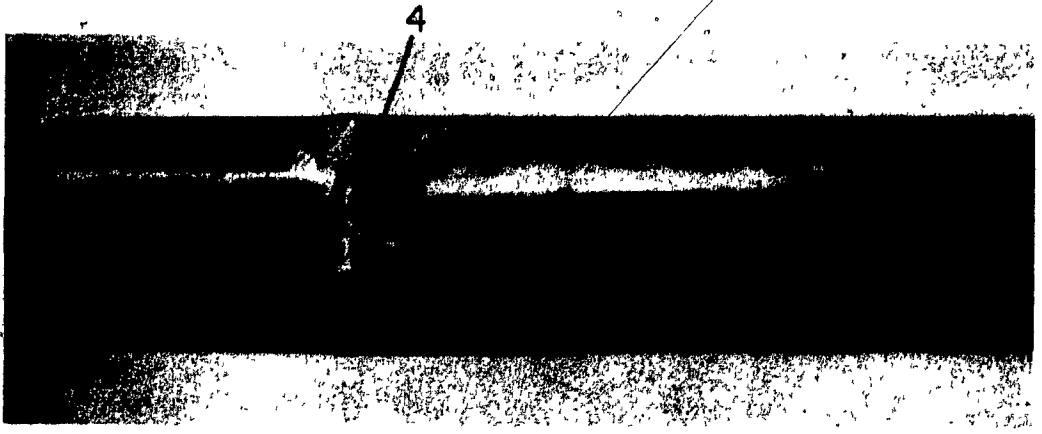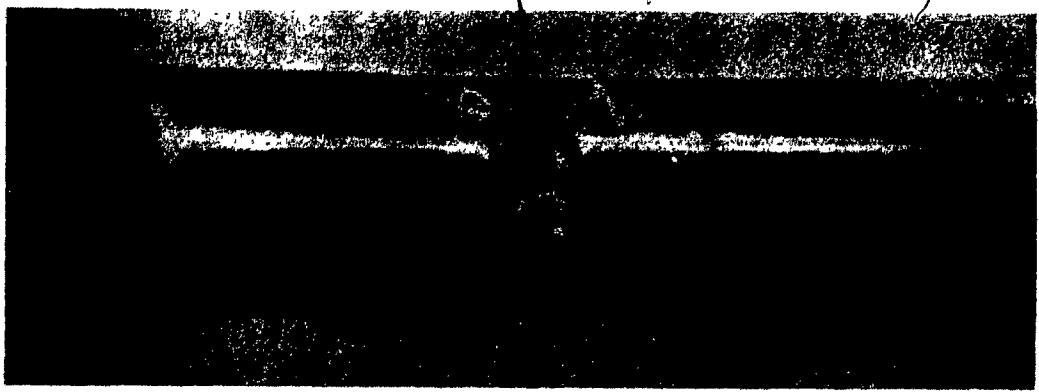
total velocity pressure calculation, while two lateral holes measured P_2 and P_3, the yaw angle pressures which were also used to calculate the stream static pressure; the other lateral holes measured P_4 and P_5, the pitch angle pressures. All tappings were 0.8 mm in diameter.

An individual calibration was supplied for this probe by United Sensors and Control Corporation, which had been obtained in their wind tunnel at velocities similar to those expected to be encountered in this study. This calibration chart is shown on Figure 6 and the procedure for the calculation of the velocity components is described in detail in the Appendix. It is claimed that this type of probe can be used up to Mach 0.7.

References (23, 24) stated that an $(Re)_d$ of 30 (Reynolds number where the measurement hole diameter on the probe is the characteristic size) is the minimum value for which viscous effects are negligible. At lower $(Re)_d$ the indicated impact pressure becomes higher than the actual stream impact pressure due to these effects. This condition was satisfied for fluid velocities as low as 1 m/s for the yaw angle and total pressure tappings.

The other restriction was that the cross-sectional area of the probe should not exceed 1% of the total flow area to avoid static pressure measurement interferences. Comparing the size of

FIGURE 6

CALIBRATION CURVES FOR THE FIVE-CHANNEL PRESSURE PROBE

CALIBRATION DATA FOR TYPE DA & DAT 3-DIMENSIONAL DIRECTIONAL PROBES

θ: PITCH ANGLE

| −50° | −40° | −30° | −20° | −10° | 0° | +10° | +20° | +30° | +40° | +50° |

$$\frac{P_4 - P_5}{P_1 - P_2}$$

PITCH ANGLE PRESSURE COEFFICIENT
VS. PITCH ANGLE

VELOCITY PRESSURE COEFFICIENT
VS. PITCH ANGLE

.80

.60

.40

.20

0

−.20

−.40

−.60

−.80

1.30

1.20

1.10

1.00

.90

.80

.70

.60
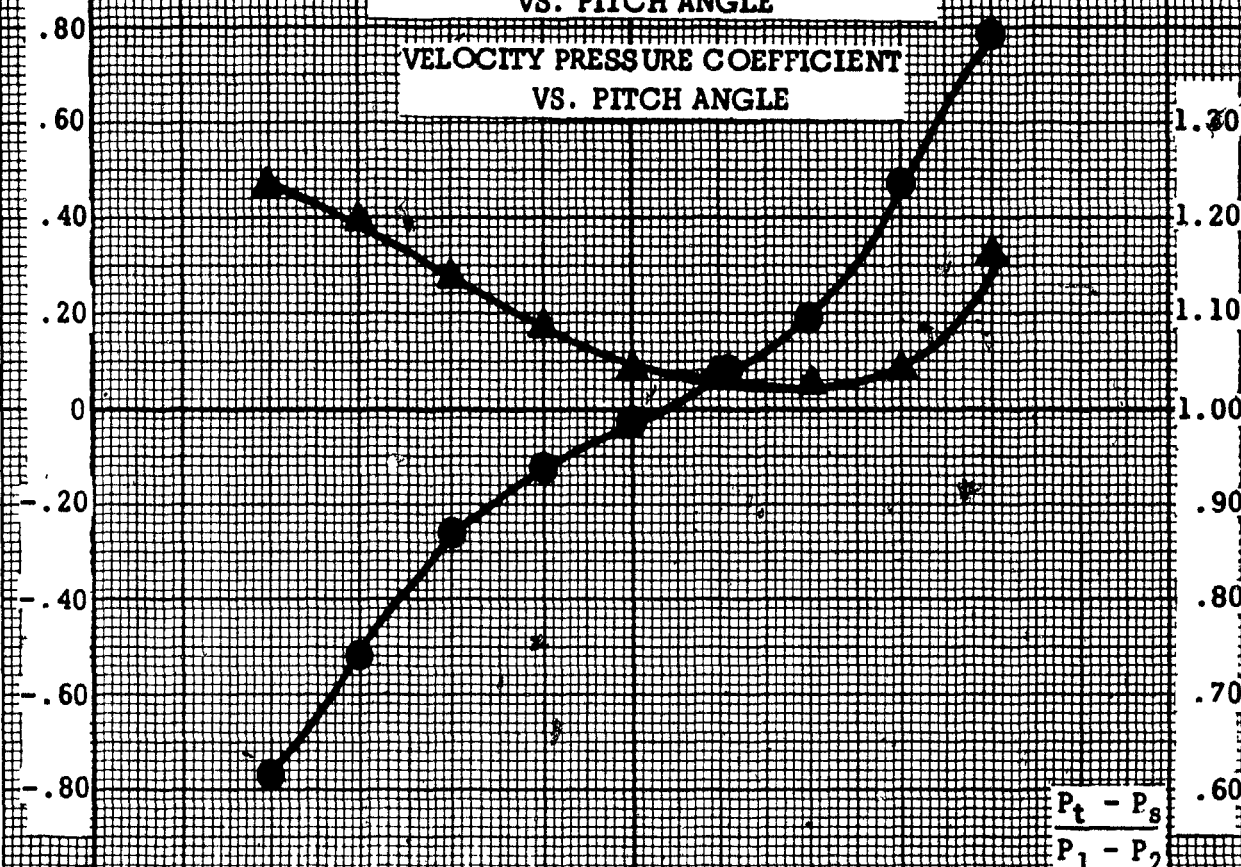
$$\frac{P_t - P_s}{P_1 - P_2}$$

$$\frac{P_1 - P_t}{P_t - P_s}$$

TOTAL PRESSURE COEFFICIENT
VS. PITCH ANGLE

0

−.10
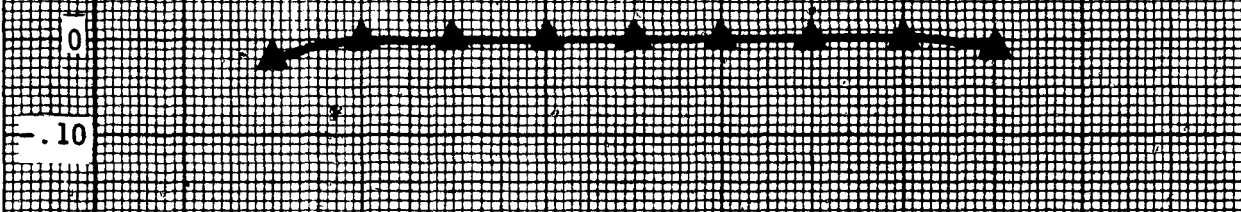
P_t : TOTAL PRESSURE
P_s : STATIC PRESSURE
P_1 : INDICATED TOTAL PRESSURE
P_2 : INDICATED STATIC PRESSURE
P_4, P_5 : PITCH ANGLE PRESSURES
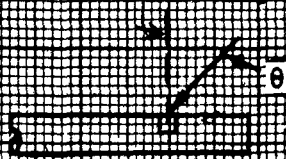
UNITED SENSOR & CONTROL CORP.

WATERTOWN · MASS

$$M_r : \frac{P_1 - P_2}{P_1 \text{ abs.}}$$

θ

PROBE TYPE: *DA-250*
SERIAL NO.: *B-134*
DATE: *5-2-77*
CALIB. BY:

the chamber (1.7 m in height and a smallest diameter of 0.2 m) a

probe of 6.4 mm diameter should not perturbate the flow pattern

noticeably or increase local static pressures. Pitch angle

effects are unavoidable for measurements very near the wall, as

explained in references (25, 26) for all pressure probes, but

correction charts are available for most of the simple cases.

The pressure responses of the five channels were fed to

the scanning valve and U-tube manometers described below, through

five 3.2 mm (0.125 in) diameter vinyl tubings.

Traverse Unit

The measuring probe was mounted on a manual traverse

unit made by United Sensor and Control Corporation, model C-100-48,

with a collet which locked it firmly in position without danger of

denting the stem. This system is shown on Figure 7. The position

of the centre measuring hole of the probe was measured on a scale

graduated in divisions of 0.1 in (0.254 cm) and a vernier with

accuracy of 0.01 in (0.0254 cm). The scale length was 122 cm

(48 in). The lock could be locked firmly at any position.

FIGURE 7

PHOTOGRAPH OF THE HORIZONTAL POSITION

AND ANGLE VERNIERS

Measurement of Angles

The angle of rotation of the probe, which was equivalent
to the yaw angle, was measured in increments of $0.2°$ over a full
$360°$ on a protractor graduated in $2°$ divisions for easy read-
ability and a large scale vernier with $0.2°$ divisions. Both
vernier and protractor were friction-loaded with adjustable
springs and balls. Easy and accurate rotation for any angle was
obtained. The vernier was adjustable, permitting the zero angle
point to be set at any time without loosening the probe in the
collet and losing the distance setting.

Vertical Positioning

The entire system was mounted on a heavy-duty high-
speed camera tripod which was equipped with adjustment of angle
with respect to horizontal level around two axes, and vertical
positioning for nearly all positions required in the experiments.
The entire set-up is shown on Figure 8. For the measurements
at the two lower ports a smaller tripod was used.

FIGURE 8

PHOTOGRAPH OF THE PROBE'S SUPPORTING SYSTEM

Pressure-Averaging Choke

This is a device manufactured by United Sensors and Control Corporation, with the denomination USC-8261-3, which receives as input two different pressures and its output is the average of those pressures. All signals are pneumatic.

The probe was aligned with the flow by turning the protractor and the yaw angle of the probe was thus changed until P_2 = P_3 was attained. Then, the pressure-averaging choke decreased the oscillations in P_2 by averaging it with P_3, resulting in a pressure P_2' for measuring the differential of this pressure with other pressures. The degree of accuracy was increased very much by the use of this device.

Fluid Wafer Switch

This switch permitted the measurement of differential pressures between two tappings of the probe or between one of the tappings and the atmospheric pressure, according to the switch positioning. It was made by Scanivalve Inc., under the specification WO601/2P-6T, and was equipped with a hand-drive of specification WNOB 12.

A simplified diagram of the pressure scanner is shown on Figure 9. A few examples will explain its operation: at position 1, pressure P_1 is connected to one port of the transducer (x), while P_{atm} is connected to the other reference (r) side. The differential

FIGURE 9

DIAGRAM OF THE PRESSURE-SCANNING VALVE
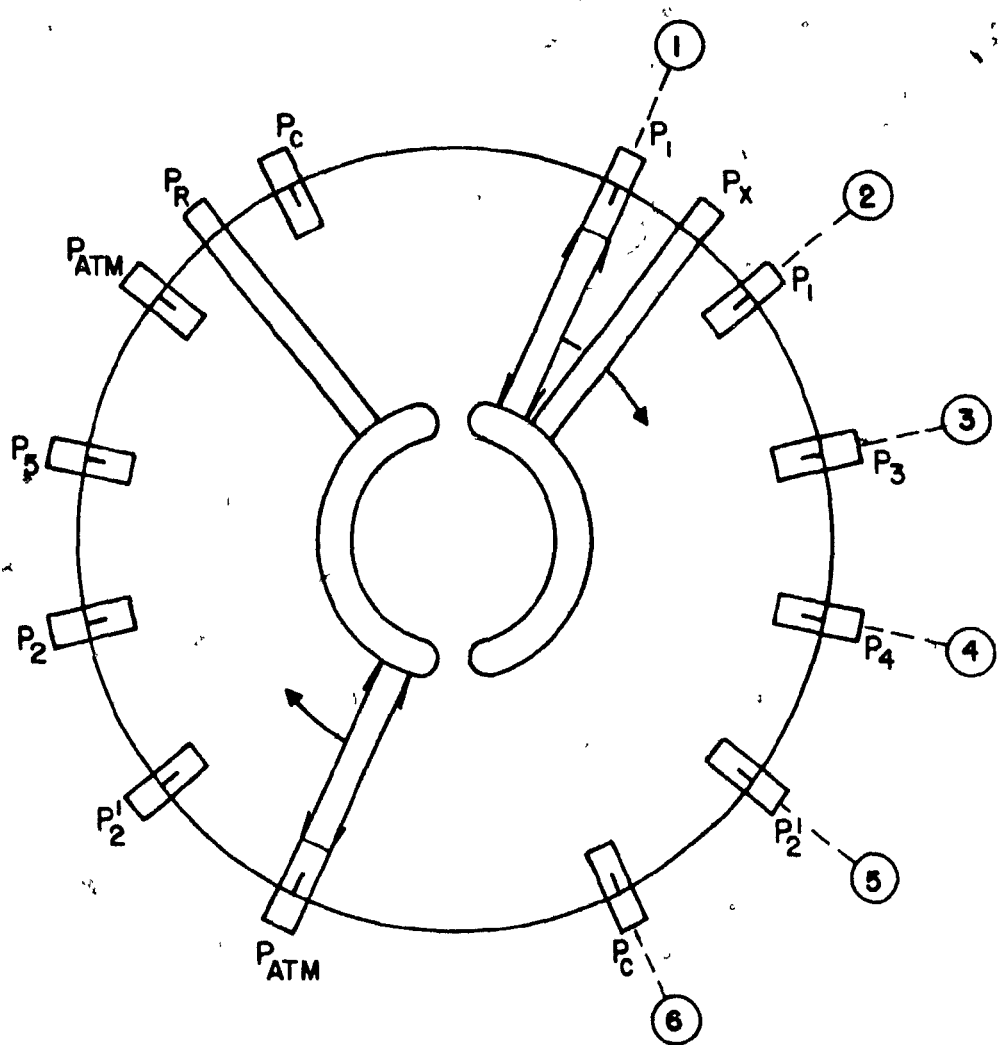
POSITION	DIFFERENTIAL PRESSURE MEASURED ($P_X - P_R$)
1	$P_1 - P_{ATM}$
2	$P_1 - P_2'$
3	$P_3 - P_2$
4	$P_4 - P_5$
5	$P_2' - P_{ATM}$
6	$P_c - P_c = 0$

pressure $(P_1 - P_{atm})$ is then read on the electronic pressure meter. In position 2, the transducer reads $(P_1 - P_2')$. In position 6, it reads a differential pressure of zero because the ports of the transducer head are interconnected and the pressure on both sides of the membrane is P_c. This last position was used for the calibration of the transducer.

Pressure Transducer

The differential pressure selected by the scanning valve was measured on a pressure transducer when it was lower than its maximum range of 3 mm Hg. Higher pressures were measured on methanol-fitted U-tube manometers.

The transducer was manufactured by MKS Instruments, Inc., and specified as MKS BARATRON TYPE 77 ELECTRONIC PRESSURE METER using a TYPE 77H-3 PRESSURE HEAD and a TYPE 77M-XR PRESSURE INDICATOR. It is shown on Figure 10.

This pressure meter was a precision instrument that measured low pressures and vacua with an accuracy equal to that obtained at higher pressures. The instrument provided a five-place digital, null-balance readout for higher precision. True pressure (force per unit area on diaphragm) is measured, rather than ionization or thermal equivalents of pressure.

The pressure scanner outlet tubes were connected to ports P_x and P_r, with the normally higher pressure at P_x. This provided

FIGURE 10

PHOTOGRAPH OF THE SCANNING-VALVE, PRESSURE MEASURING HEAD, ELECTRONIC PRESSURE INDICATOR AND U-TUBE MANOMETERS

positive readings. The accuracy was generally good enough for the purposes of this investigation to use the panel indicator instead of the digital readout for reading pressure differentials.

The equipment was verified for zero and full-scale stability before and during operation and the necessary adjustments were made where small deviations occurred at the lower range scales using a balancing system incorporated in the instrument. For this, the pressure scanner was used at position 6, i.e., the transducer ports P_x and P_r' were interconnected, as stated before.

U-Tube Manometers

Two U-tube manometers filled with Methanol (density = 0.79 g/cm^3) were installed for the measurement differential pressures $(P_1 - P_{atm})$ when they were higher than 3 mm Hg, which were observed for the higher inlet velocities.

OPERATING PROCEDURE

Orifice Calibration and Flow Rate Measurements

The orifice discharge coefficient is significantly affected by flow disturbances originating in bends, valves and other fittings located upstream from the orifice. As a general rule, the orifice plate should be placed 50 pipe diameters downstream and 10 pipe diameters upstream from any disturbance. Since these conditions could not be met in the present experimental set-up, a calibration

of the orifice against pitot tube measurements was necessary. The
pressure probe used for the vortex flow measurements was also used
for this purpose. A straight probe cantilevered out from the wall
away from the boundary layer causes a flow distortion showing up
as a secondary flow along the axis and around the tip. A local ac-
celeration in flow is thus created near the tip of the probe which
increases as the tip approaches the opposite wall. This causes a
static hole located near the tip to show a steadily dropping static
pressure as the probe is traversed from one wall to the other. A
calibration chart correcting for these effects was obtained specif-
ically for the probe used in this study from United Sensors and
Control Corporation through measurements in a section of the same
size as the tubing where the traverse was performed, and it was
used in the orifice flowmeter calibration procedure.

A ten-point traverse was made across the duct in a straight
section of the outlet line from the blower, between the blower and
the orifice, from which the average velocity in the duct, and hence
the volumetric flowrate to the chamber, were calculated. (Fig. 11)

The local velocity was calculated from the following
equation:

$$V = 23.94 \sqrt{(P_T - P_S) \cdot T/P_{atm}} \tag{24}$$

Flow Visualization

In order to visualize qualitatively the direction and

FIGURE 11

ORIFICE FLOWMETER CALIBRATION CURVE
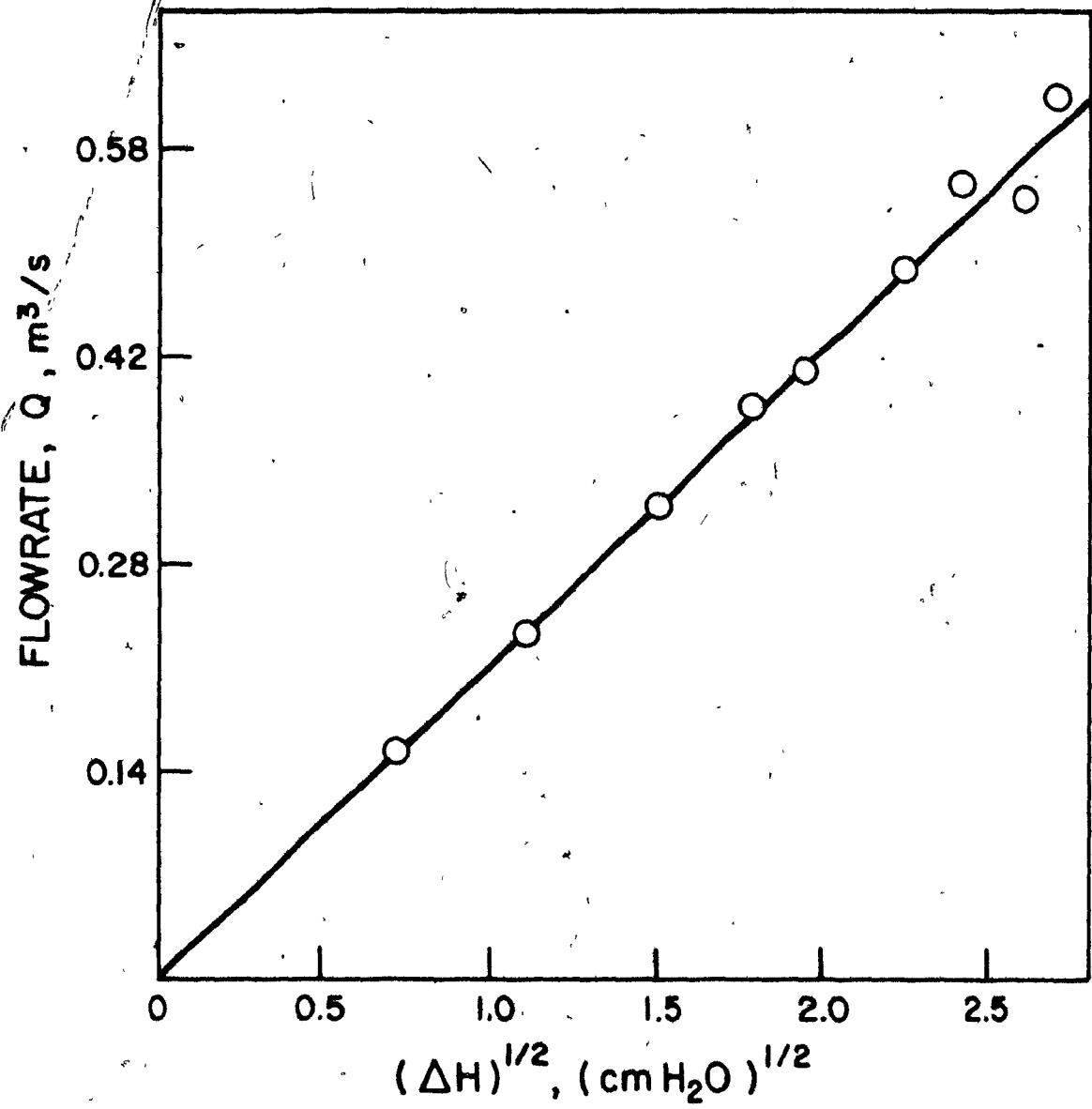
pattern of flow, small wool tufts fastened to the heads of 3/16 in (0.476 cm) diameter stainless steel rods were used. It has already been mentioned that it was necessary to know the main direction of the flow for the proper positioning of the probe. This was particularly important near the centre of the chamber, where reverse axial flow occurred.

MEASUREMENTS WITH THE FIVE-CHANNEL PRESSURE PROBE

Prior to an experiment, the pressure meter and the regulating heating system for the pressure head were both switched on. These were warmed up for half an hour. Then, full-scale and zero adjustments were made, while the pressure head ports were interconnected. The probe was then inserted in the vortex chamber through the seal which was threaded on the particular port being studied. The probe supporting system was next checked for probe horizontal levelling with a spirit level. With a plumb line inserted through a port installed in the roof of the chamber, exactly at the axis position, it was verified whether the probe was inserted in a truly radial direction, following which the plumb line was removed.

The five-channel pressure probe was now ready for measurements. The blower was switched on, the flow rate was controlled with the butterfly valves at the outlet of the blower and the angle of inlet was adjusted with the inlet vanes. When stable flow conditions were reached, the radial traverse was begun. For each

single velocity-static pressure measurement the probe was positioned radially and its position measured on the linear scale vernier of the traverse unit, which could be read accurately to 0.01 in (0.0254 cm). The scanning valve was set at position 3. At this position the differential pressure $(P_3 - P_2)$ was read on the transducer system using the scale with the highest readable deflection. The protractor of the probe was then rotated until $(P_3 - P_2)$ read zero. A smaller scale on the pressure meter was selected and the angle of the probe changed until the movements of the needle were negligible for all available scales. The angle of the flow (ψ) could now be read directly from the protractor with an accuracy of 0.2°. At this fixed angle, the scanning valve was set at all other positions and the respective differential pressures were registered. If a differential pressure was larger than 3 mm Hg, which only occurred for the measurements of $(P_1 - P_2)$, $(P_1 - P_{atm})$, and $(P_2 - P_{atm})$, it was read on the methanol-filled U-tube manometers. Figure 12 shows the agreement between the results obtained from the transducer and the ones obtained from U-tube manometers. For every measurement, the temperature in the chamber and the barometric pressure were noted.

At any axial location, measurements had to be performed for at least twenty-five radial positions for each condition of flow rate and inlet flow angle. This large number of measurements was necessary because of the large variations in the axial velocity component and in flow angle along a radial traverse.

FIGURE 12

COMPARISON BETWEEN THE DIFFERENTIAL PRESSURES MEASURED

WITH THE TRANSDUCER AND THE U-TUBE MANOMETERS
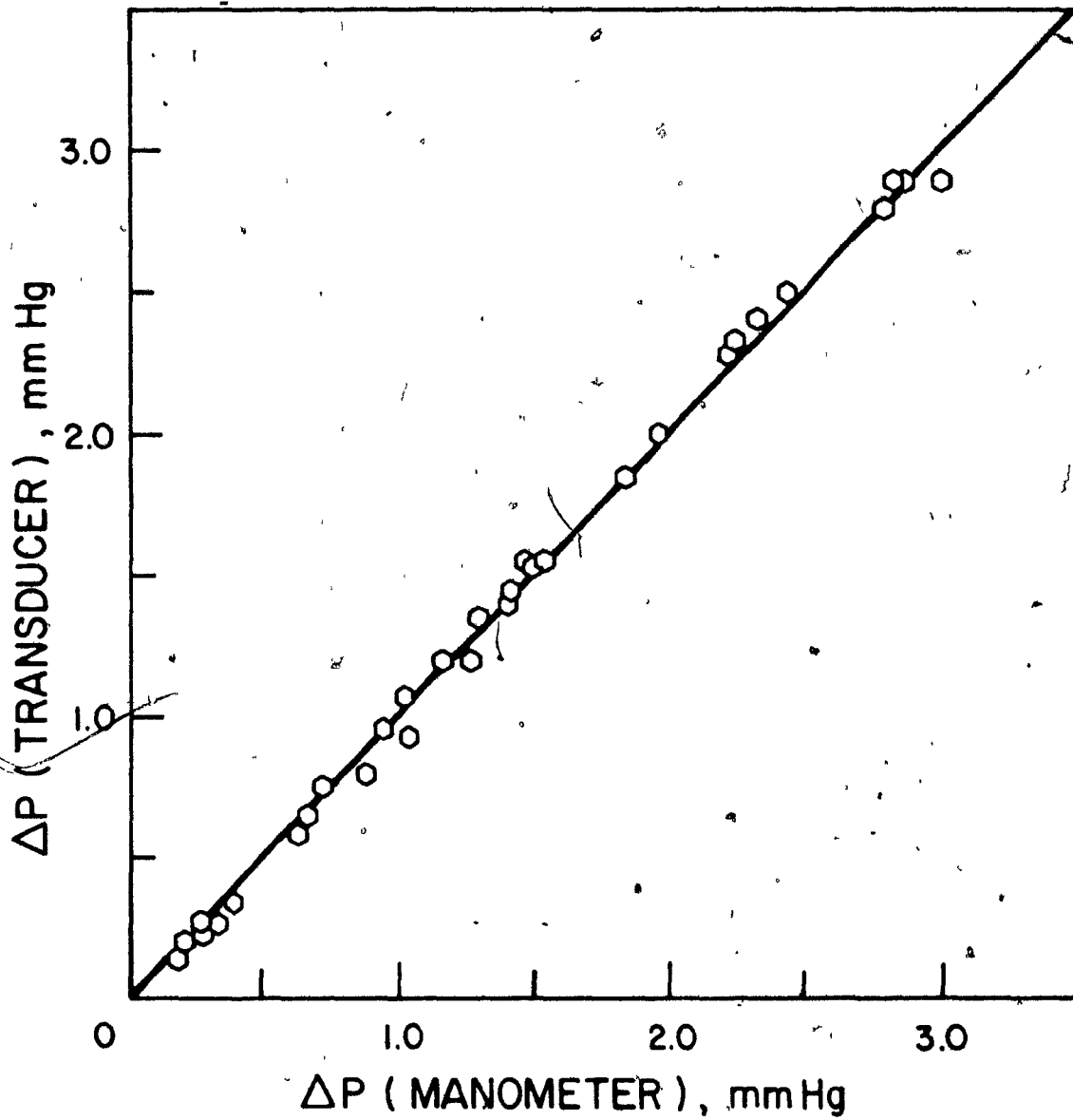
In experiments of this kind, which involve a large number of variables, the number of experiments increases very rapidly with the number of levels chosen for each variable. An experimental design method was used (27) to choose the number of levels for each variable that would represent best the effect it has on the vortex flow pattern, without requiring a prohibitively large number of experiments.

In the Appendix, the method used for the calculation of the velocity components and of the static pressure is explained. A small programable desk calculator proved to be very useful in this case, where three different curves gave calibration factors as functions of intermediate results of the calculations. After being read from these curves, these factors were used for further processing.

When the probe was aligned with the flow by yawing it until $P_2 = P_3$, the velocity pressure $(P_T - P_S)$ and the direction of the velocity vector relative to the probe were calculated from the following equations:

$$\theta = C \ (P_4 - P_5) \ / \ (P_1 - P_2) \tag{22}$$

$$(P_T - P_S) \ / \ (P_1 - P_2) = K \ (\theta) \tag{23}$$

$$(P_1 - P_T) \ / \ (P_T - P_S) = F \ (\theta) \tag{24}$$

where $\underline{C}$, $\underline{K}$, $\underline{F}$, are the calibration factors of the five-channel pressure probe, read from the calibration chart shown on Figure 6.

It should be noted that the curve for $F(\theta)$ is horizontal and stays at zero for the range of θ from $-30°$ to $+30°$. This indicates that P_1 is equal to P_T for this range of θ and no error would result if the value of θ were not accurately measured. The sensitivity of $K(\theta)$ to an inaccuracy in the measurement of θ is also very small.

Due to its very small size, the pitch angle, θ, the angle of deviation of the velocity vector from a constant radius path, could not be obtained accurately. The differential pressure $(P_4 - P_5)$ used to calculate this angle oscillated within a certain range and the average between the maximum and minimum values was used. As already discussed before, the error resulting from this procedure is small, due to the relatively small sensitivity of the calibration factors to the pitch angle, for the ranges of θ encountered in our experiments. The only velocity component for which calculation was hampered by this inaccuracy was the radial velocity (u). For $(P_T - P_S)$, the maximum possible error was 8%.

The magnitude of the velocity vector was obtained from equation (21). Its velocity components were obtained from the geometrical relationship shown on Figure 13.

When the probe was aligned with the flow, after being yawed by an angle ψ, the vector velocity could be decomposed into its three components u, w, and v, as given by:

FIGURE 13

DIAGRAM OF THE RELATION BETWEEN THE VECTOR VELOCITY

AND ITS COMPONENTS FOR FIVE-CHANNEL PROBE MEASUREMENTS

RELATION BETWEEN MEASURED VELOCITY VECTORS, ANGLES OF FLOW AND VELOCITY COMPONENTS
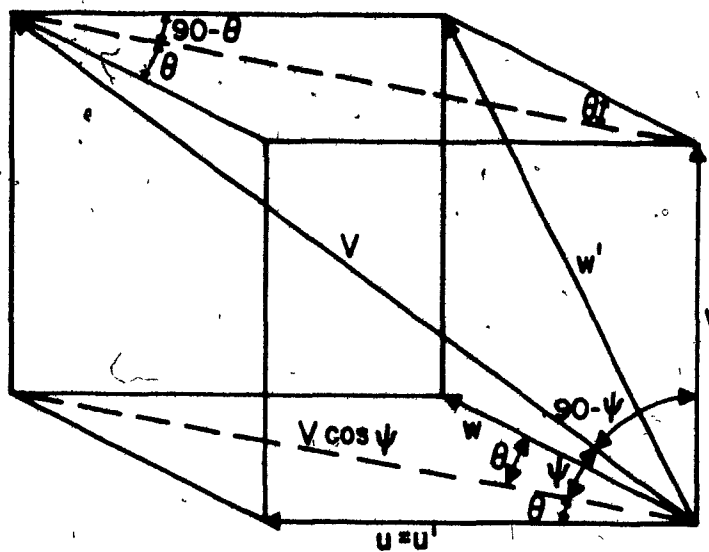
$$u = V \sin \theta \qquad (25)$$

$$v = V \sin \psi \cos \theta \qquad (26)$$

$$w = V \cos \psi \cos \theta \qquad (27)$$

The static pressure relative to the atmospheric pressure was found from:

$$P_S - P_{atm} = -[(P_1 - P_T) + (P_T - P_S) - (P_1 - P_{atm})] \qquad (28)$$

where $(P_1 - P_T)$, $(P_T - P_S)$, and $(P_1 - P_{atm})$ were obtained from Equation (24), Equation (23) and direct measurement, respectively.

RESULTS AND DISCUSSION

VARIATIONS OF FLOW VARIABLES WITH POSITION

i) Tangential Velocity

The profiles for the tangential velocity showed clearly the existence of two main flow regions, namely, a forced-vortex near the axis of the chamber and a free-vortex in the main part of the flow. This can be observed in Figure 14, which presents the radial profile of tangential velocity for different axial positions, maintaining the inlet velocity constant at 8.6 m/s and the inlet flow angle at $0°$. It can be seen that the pattern of flow is the same for all vertical positions.

FIGURE 14

EFFECT OF AXIAL POSITION ON THE

TANGENTIAL VELOCITY PROFILES

INLET VELOCITY = 8.6 m/s

INLET ANGLE = 0°

Figure showing TANGENTIAL VELOCITY (m/s) versus r/R for various ports.

INLET VELOCITY = 8.6 m/s
INLET ANGLE = 0°

PORT
10
9
7
6
2
3
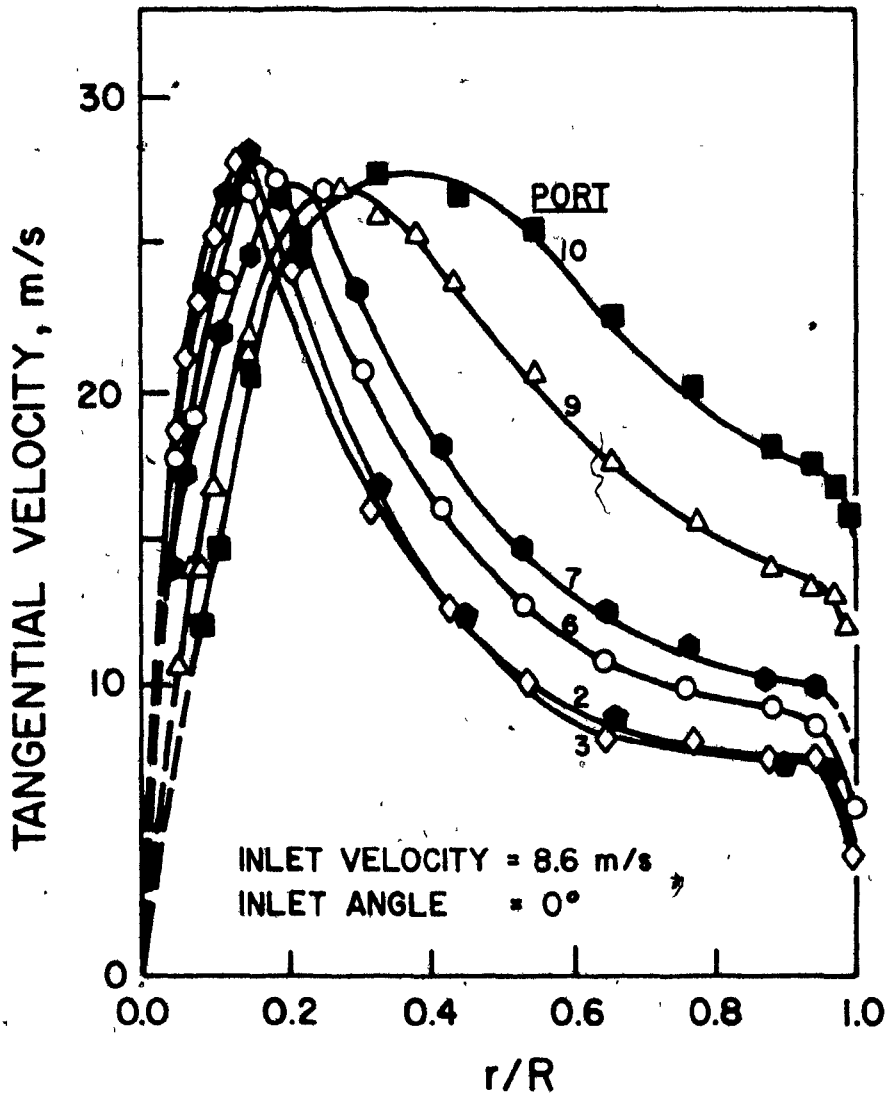
In the lower regions of the conical chamber, in which the radius is obviously smaller, Figure 14 clearly indicates a shift of the dimensionless radial position $(r/R)_{max}$, at which the maximum tangential velocity occurs. However, the actual radius $(r)_{max}$, where this maximum occurs stays relatively constant and seems to be independent of the axial position. The mean value of this radius is $(r)_{max} = 7.2$ cm, with a standard deviation of $s = 0.8$ cm. The probable reason for this deviation is the small degree of asymmetry in the flow imparted by the single inlet, and it can be inferred that the radial position of maximum tangential velocity would be constant if the flow was truly symmetrical. As a result, the free-vortex region in the lower part of the cone is relatively smaller than for positions with larger radius higher up in the chamber.

Extrapolating the velocity profiles to positions near the wall, without accounting for boundary layer effects, the extrapolated tangential velocity for port 6 was found to be approximately equal to the inlet velocity to the chamber.

At the lower stations, the flow accelerated due to the smaller radius and at the higher stations the tangential velocity near the walls was lower than the entrance velocity (the inlet velocity to the chamber was calculated by dividing the total flow rate measured at the calibrated orifice flowmeter by the total inlet cross sectional area, 480 cm^2).

.The velocity profile for port 2, located on the cyl-
indrical portion of the chamber, had the same characteristics as
for the other ports and is very similar to the profile for port
3, the nearest port in the conical section. From this, it can be
concluded that the different chamber geometries, cylindrical or
conical, do not affect the shape of the tangential velocity
profile.

ii) Static Pressure

Figure 15 presents the effect of axial position on the
static pressure profiles for constant inlet flow angle and velocity
into the chamber (0° and 8.6 m/s, respectively). A negative static
pressure relative to the atmospheric pressure is observed near the
axis of the vortex. For a particular axial position, the pres-
sures are larger near the wall of the chamber due to the action of
the centrifugal forces.

It can be observed that, generally, lower static pres-
sures occur at lower axial positions. The dimensionless radial
position (r/R) where the static pressure becomes negative was noted
to increase for lower positions in the chamber, where the radius of
the chamber decreased. This should cause reverse flows (upwards
in the chamber) near the axis. These results were confirmed by
axial velocity measurements, which are reported in the next section.

FIGURE   15

EFFECT OF THE AXIAL POSITION ON THE

STATIC PRESSURE PROFILES

INLET VELOCITY = 8.6 m/s

INLET ANGLE = 0°

PORT
3
6
9
10

INLET VELOCITY = 8.6 m/s
INLET ANGLE = 0°

STATIC PRESSURE ($P_s - P_{atm}$), mmHg

r/R
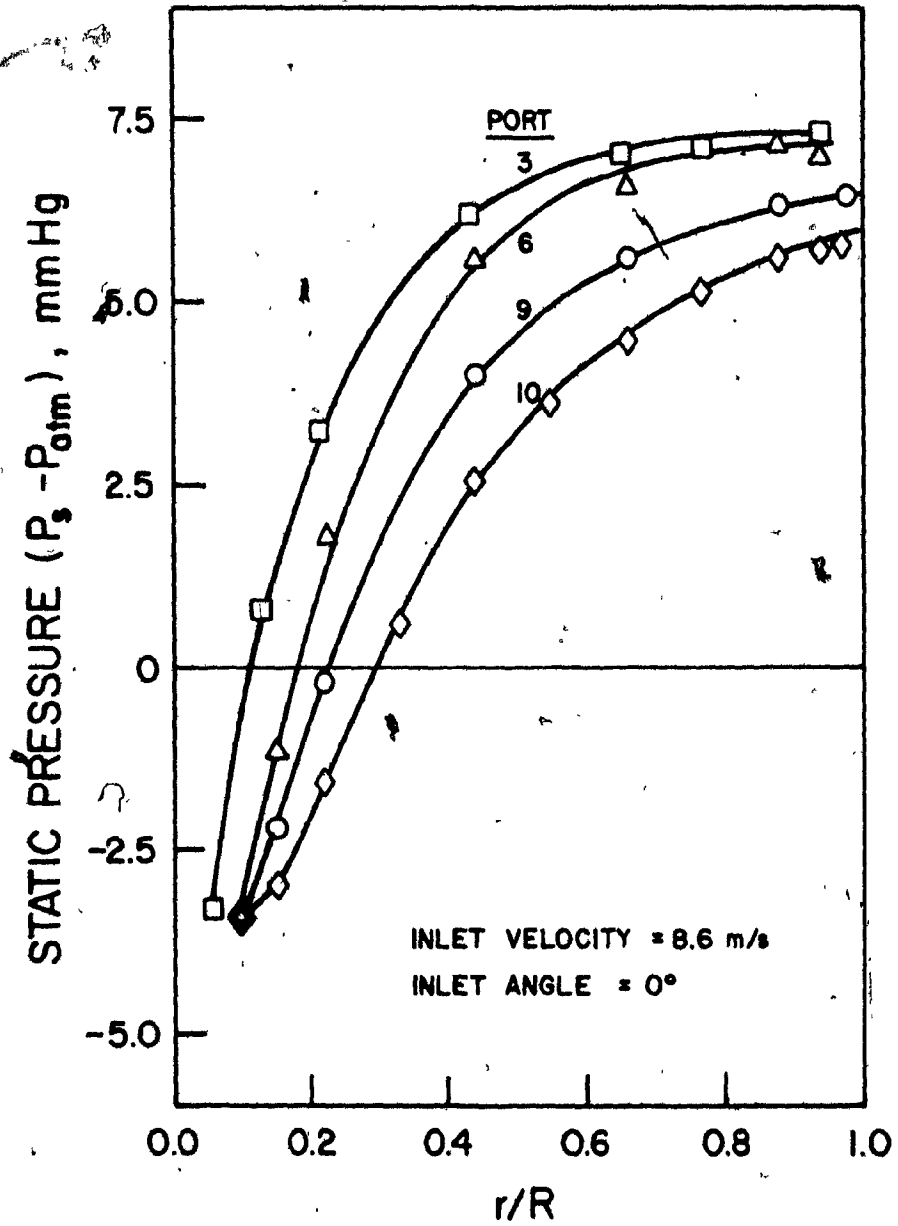
iii) Axial Velocities

Radial profiles of the axial mean velocities for port 9 are shown in Figure 16, for an inlet velocity of 8.6 m/s and an inlet angle of 0°. Although the measurements in the region near the centreline of the chamber were very difficult due to a high degree of turbulence observed in this region, the results showed clearly that a reverse flow occurred in this region. This was confirmed by the static pressure measurements discussed above and, at least qualitatively, by flow visualization. In Figure 16, this flow reversal is shown by the negative axial velocities measured in the axis region. It can be noted that a strong asymmetry existed for the axial velocity profile. The single tangential entrance in the vortex chamber caused the formation of preferential paths for the secondary flows. Consequently, the reverse flow was also asymmetric.

Comparing Figure 16 with Figure 14, it can be seen that the tangential velocities were always much larger than the axial velocities, and being characteristic of the vortex flow, the tangential velocity profiles were of a more symmetric nature, while the axial velocity profiles were deformed by the secondary flows. It should also be noted that the maximum axial velocities occurred in the region of maximum tangential velocities, and that the axial velocities were relatively high near the walls.

The axial velocity profiles' measurements were checked by

FIGURE 16

AXIAL VELOCITY PROFILE FOR PORT 9

INLET VELOCITY = 8.6 m/s

INLET ANGLE = 0°

PORT 9

INLET VELOCITY=8.6m/s
INLET ANGLE=0°
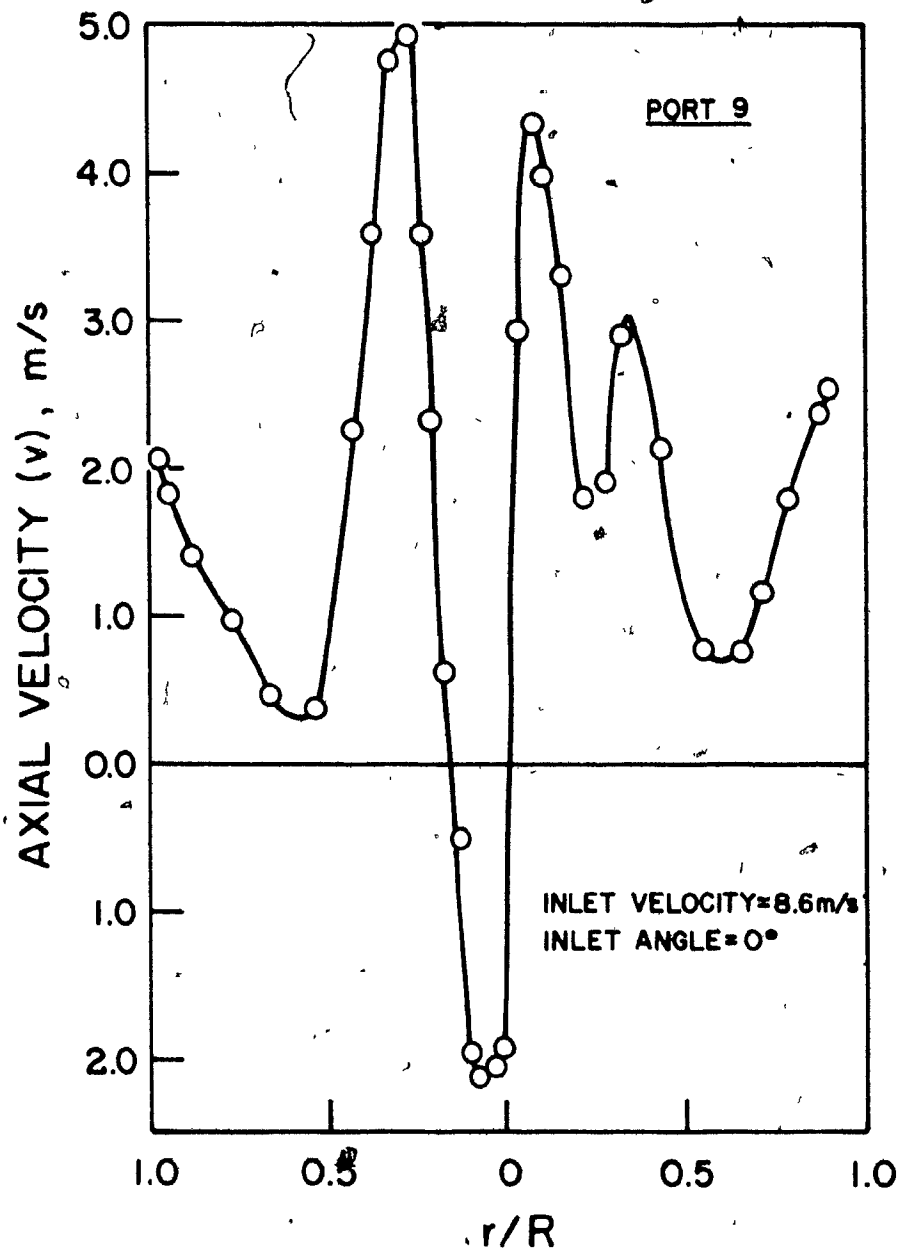
installing a new port (No. 6') on the chamber at a position
diametrically opposite to port 6, and comparing the axial velocity
profiles measured from the two sides. The profiles measured by
inserting the probe from the opposite sides agreed satisfactorily
and the asymmetry was confirmed.

The axial velocity profiles found in this work disagree
with the ones reported in Reference (3), for different inlet
conditions and a small diameter outlet. In this reference, the
profiles obtained increased exponentially with the radius and the
maximum was reached near the wall of the chamber. However, the
profiles reported in References (12, 13, 15) all follow the same
pattern as observed in this work.

In Figure 17, a comparison of the axial velocities for
two different axial positions is shown. It can be noted that the
axial velocities are larger at the lower position in the chamber
(where the chamber radius is smaller), as should be expected from
a mass balance. Mass balances could be obtained from the inte-
gration of the axial velocity profiles over the cross-sectional
area of the flow and should equal the total inlet volumetric flow
rate measured through the orifice flowmeter. The flow rate cal-
culated would be the true flow rate if the profiles were repre-
sentative of a symmetric ideal profile. Such integrations were
indeed performed but only in a few cases did the calculated flow
rate agree with the measured flow rate. Measurements and inte-
gration over complete cross sectional planes of the chamber would

FIGURE   17

COMPARISON OF AXIAL VELOCITY PROFILES

FOR DIFFERENT AXIAL POSITIONS

INLET VELOCITY = 8.6 m/s

INLET ANGLE = $0°$

Figure showing axial velocity (v), m/s versus r/R. Curves labeled PORT 9 and 6. INLET VELOCITY = 8.6 m/s, INLET ANGLE = 0°.
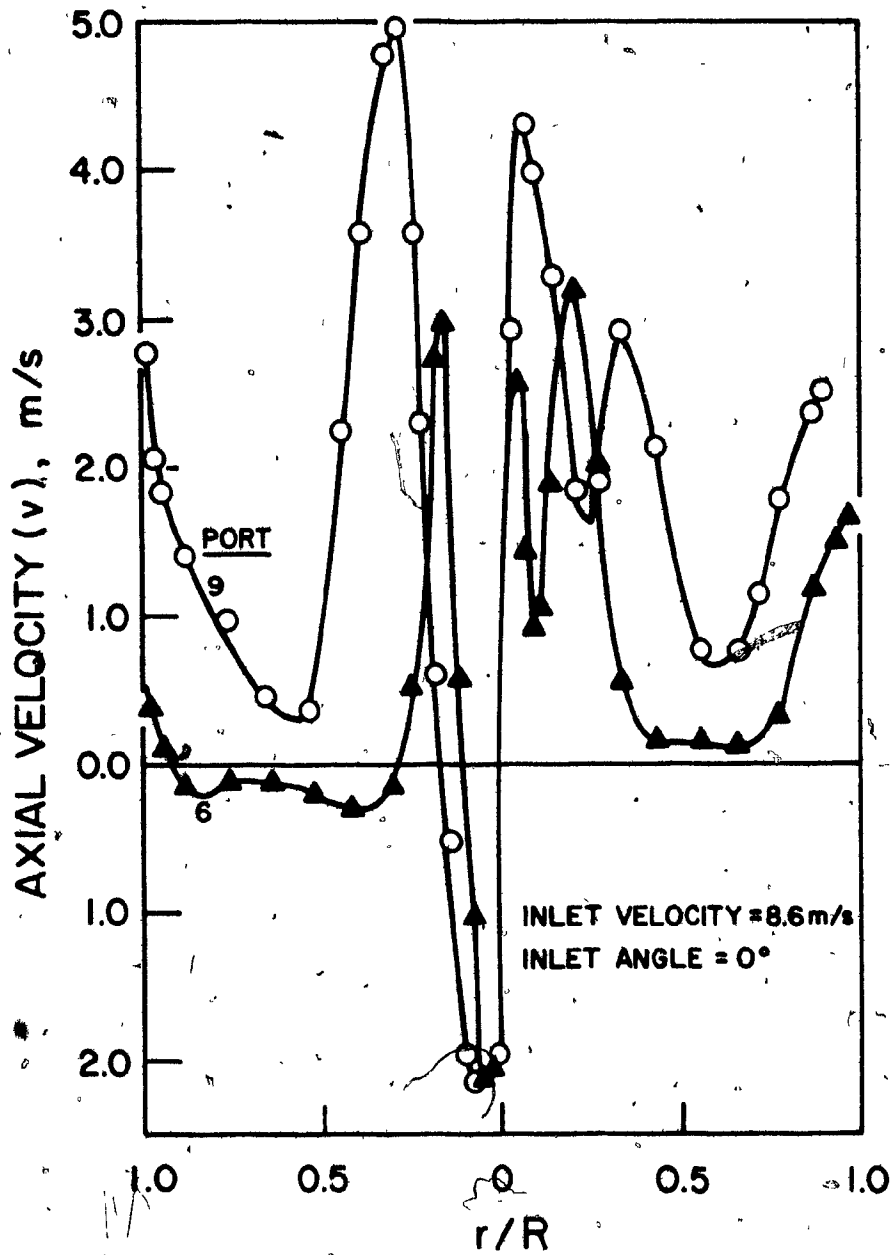
have to be performed to avoid errors caused by the asymmetry of the flow. It was not feasible in this study to install more ports to perform these measurements. From Figure 17, it can also be seen that the asymmetry is larger for port 6 than for port 9. The smaller radius at the lower position in the chamber increased the axial velocities and caused them to become symmetrical.

EFFECTS OF THE INLET VELOCITY AND FLOW ANGLE

i) Tangential Velocity

Figure 18 shows the effect of the inlet velocity on the tangential velocity profiles. As expected, the tangential component of velocity increased with the inlet velocity or air flow rate passing through the chamber. It is interesting to notice that the peak of the velocity occurs at the same (r/R) value for different inlet velocities, for the range of air flow rates used in these experiments.

One of the most striking observations made in this study was that the effect of the inlet angle on the tangential component of velocity was negligible at positions not to near the entrance. Repeated measurements and flow visualization experiments clearly indicated that although the main flow was initially deviated from its horizontal path by the directing vanes, the effect of this deviation quickly disappeared downstream as the entering air was entrained into the rotating bulk flow.

FIGURE 18

EFFECT OF THE INLET VELOCITY ON THE

TANGENTIAL VELOCITY PROFILES - PORT 6

INLET ANGLE = 0°

PORT 6
INLET ANGLE = 0°

$V_0 = 12.3$ m/s

$V_0 = 8.6$ m/s

$V_0 = 4.9$ m/s

TANGENTIAL VELOCITY, m/s

r/R
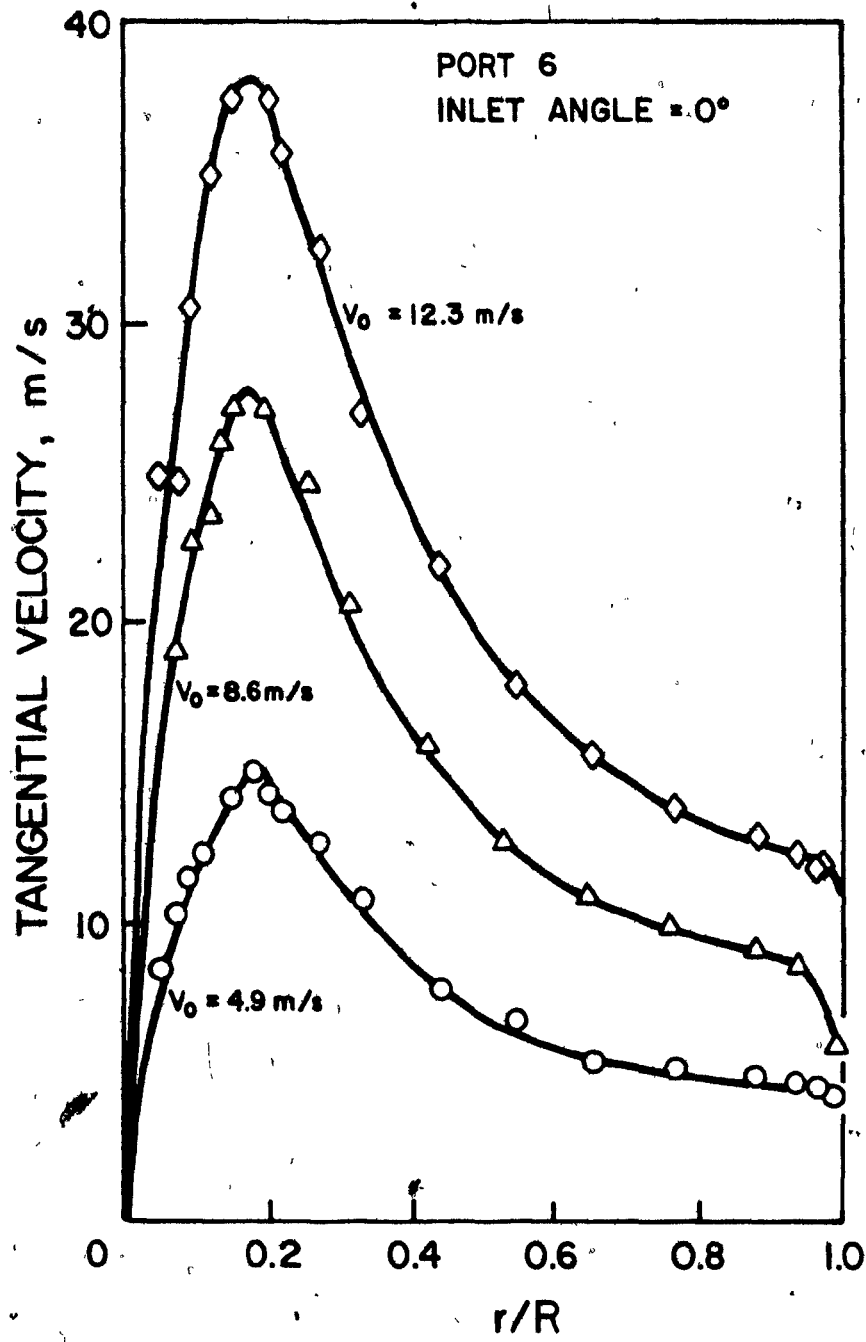
ii)   Static Pressure

Figure 19 shows the effect of the inlet velocity on the static pressure profiles. As expected, the larger inlet velocity which caused larger tangential velocities resulted in higher static pressures near the walls of the chamber. Most interesting is the observation that the inversion in static pressures always occurred at the same dimensionless radial position for each axial position in the chamber, independent of the inlet velocity. This point was in the region of the maximum tangential velocities. It was also noted that the inlet flow angle again had no influence on the static pressure profiles.

iii) Axial Velocities

Figure 20 shows the effect of the inlet velocity on the axial velocity profiles for port 6. As expected, the axial velocities are larger for larger inlet velocities. It should be mentioned that because of their much smaller values, the measurements of the axial velocities are less accurate than those of the tangential velocities and static pressures. However, the results obtained showed clearly that for the same axial position, the radial profiles of the axial velocities show a very good similarity of flow pattern for the different inlet velocities.

The inlet flow angle had a slight effect on the axial velocity profiles which is shown on Figure 21 for port 6. This axial position seemed the most representative of the conical

FIGURE   19

EFFECT OF THE INLET VELOCITY ON THE

STATIC PRESSURE PROFILES - PORT 6

INLET ANGLE = 0°

INLET VELOCITY

12.3 m/s

8.6 m/s

4.9 m/s

PORT 6

INLET ANGLE = 0°

STATIC PRESSURE $(P_s - P_{atm})$, mm Hg

r/R
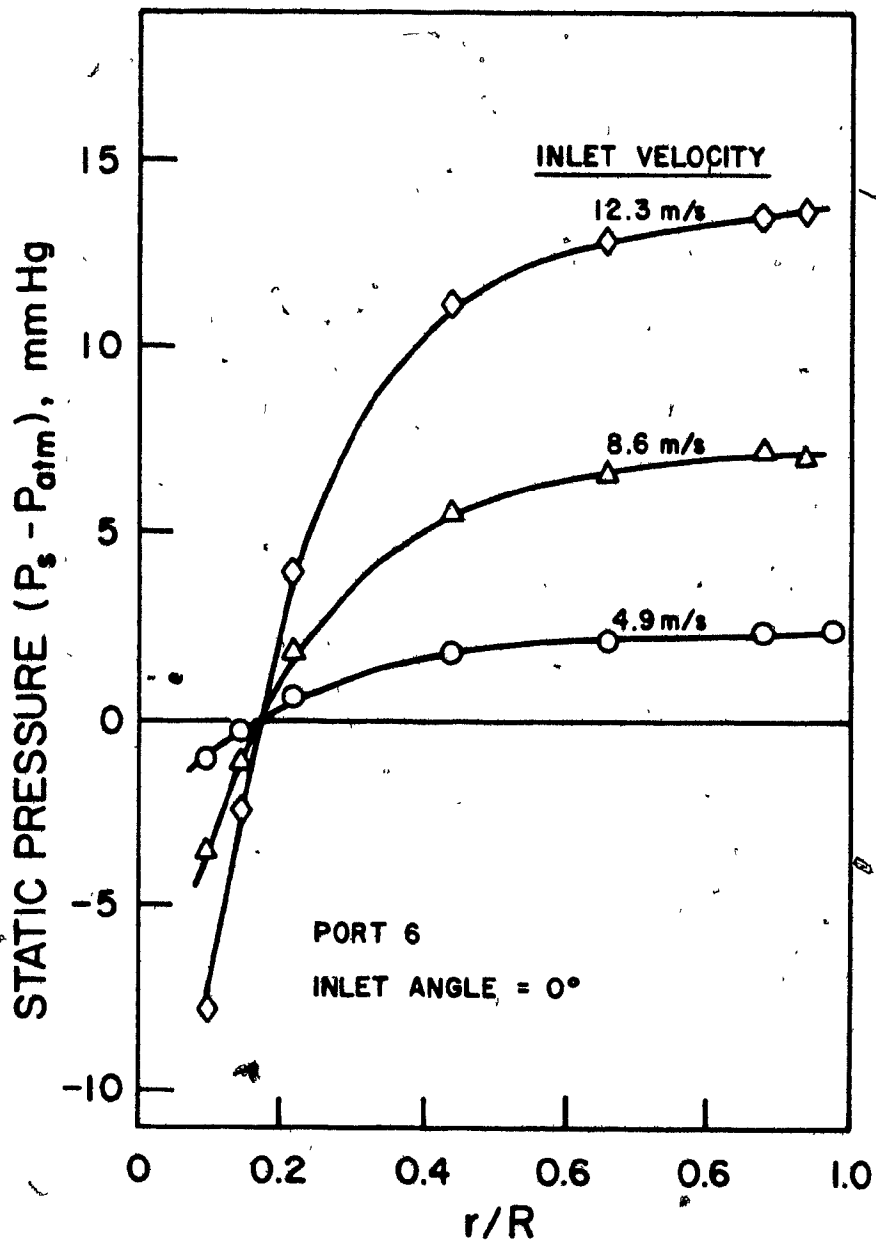
FIGURE   20

EFFECT OF THE INLET VELOCITY ON THE

AXIAL VELOCITY PROFILES - PORT 6

INLET ANGLE = 0°

(Square Symbols - 4.9 m/s Inlet Velocity
Circle Symbols - 12.3 m/s Inlet Velocity)

Axial velocity versus r/R. Plot showing INLET VELOCITY curves for 4.9 m/s and 12.3 m/s. PORT 6, INLET ANGLE = 0°.
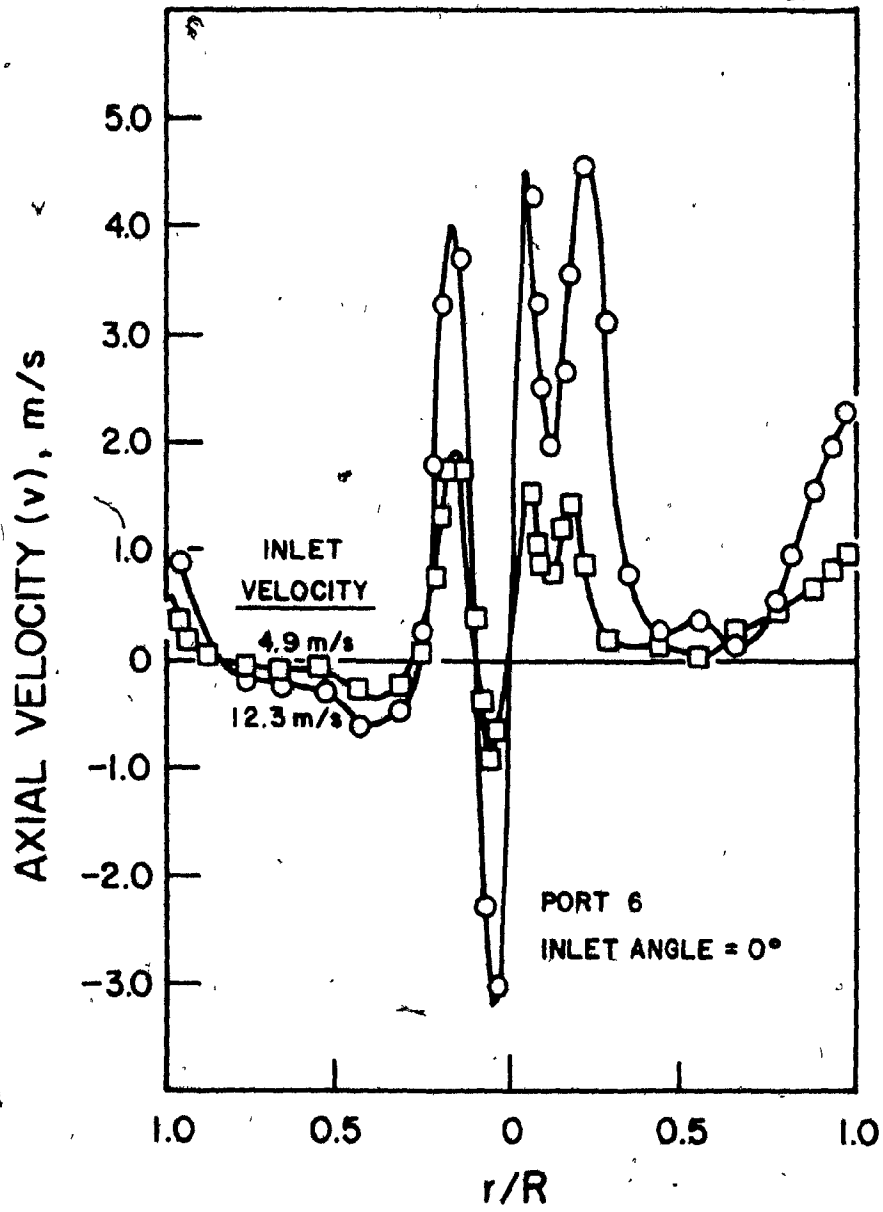
section of the chamber. Figure 21 clearly shows the distortion

in the axial velocity profile, which is enhanced near the walls

when the flow angle goes from $0°$ to $30°$. This observation is a

good proof that the flow asymmetry is caused by the entrance

conditions. Near the centreline no effect of the inlet angle was

noticed. Due to the three-dimensionality of the flow, it is

difficult to draw more conclusions about this effect without

performing many more complete traverses along different dia-

metrical directions for all axial positions. If this were done,

it is probable that a preferential spiral path could be identified

which in turn would be affected by the angle of inlet flow.

INFLUENCE ON THE OUTLET SIZE OF THE AXIAL VELOCITY PROFILES

The radical differences already reported between the work

of N. Bank (3, 14, 21) and the results of the present author, par-

ticularly in connection with the observed values of the axial

velocities and their radial profiles, prompted a close examination

of the respective operating conditions, since the two studies were

carried out in chambers of the same geometry. Outside of the dif-

ferent entrance conditions which have already been pointed out,

Bank used much smaller volumetric flow rates of entering air. He

also used a very small diameter of 7.62 cm for the chamber outlet

at the bottom. The immediate consequence of the latter would be a

considerable increase in exit velocity (everything else being

constant) and hence in the pressure drop across the exit, since the

FIGURE 21

EFFECT OF THE INLET FLOW ANGLE

ON THE AXIAL VELOCITY PROFILES – PORT 6

INLET VELOCITY = 8.6 m/s

INLET VELOCITY = 8.6 m/s

INLET ANGLE = 30°

INLET ANGLE = 0°

PORT 6

AXIAL VELOCITY, m/s

r/R
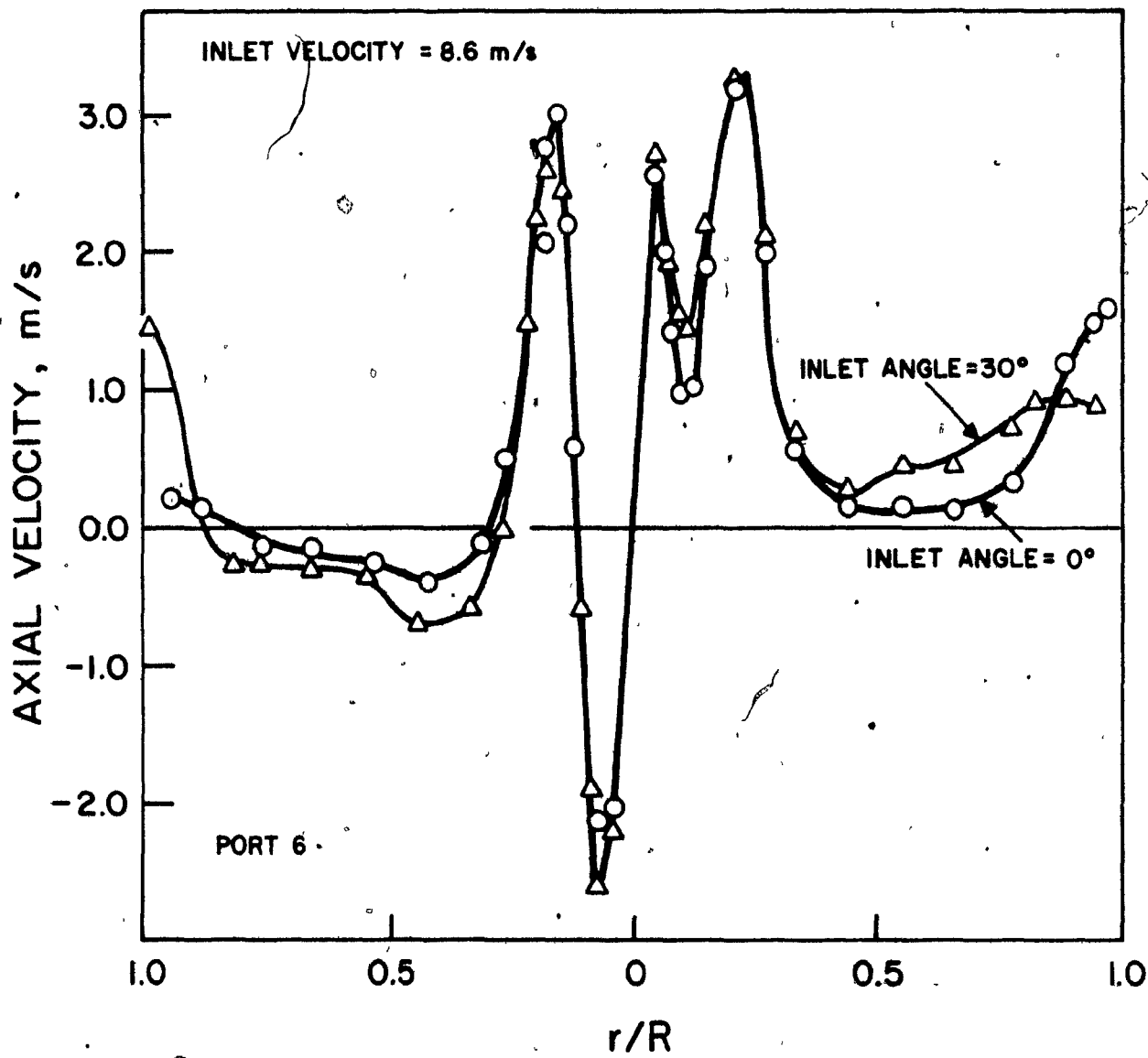
latter is proportional to the square of the exit velocity. The overall result would be an appreciable increase in the chamber's static pressure, although Bank did not measure the latter. It was therefore decided to perform additional experiments to study the effect of the outlet size on the axial velocity profiles, as it was expected that this parameter might have a good deal of influence on the axial flow behaviour.

An outlet of diameter of 7.62 cm was accordingly installed on the chamber for comparison with the diameter of 19 cm utilized in the previous experiments. Measurements were made mainly near the apex of the chamber because better symmetry of flow existed in this region (less influence of the single tangential inlet) and the axial component of velocity was relatively larger, resulting in a better accuracy in the measurements.

Figure 22 shows the axial velocity profiles for port 10, for different outlet diameters and flow rates. For 0.24 m^3/s and 19 cm outlet diameter, a central reverse flow was observed as previously noted. However, for the larger flow rates and smaller diameters studied, no upward axial flows were observed. It is interesting to note that the axial velocity profile for 0.24 m^3/s and 7.62 cm diameter outlet very nearly reaches zero at one point. In other words, a decrease in the flow rate or an increase in the outlet diameter would have caused reverse flow to occur. This pair of values could therefore be considered as a critical combination for the particular vortex chamber. From more of these combinations,

FIGURE   22

AXIAL VELOCITY PROFILES FOR DIFFERENT OUTLET

DIAMETERS AND FLOW RATES – PORT 10

PORT 10

$0.24\,m^3/s$, $D_0 = 7.62\,cm$

$0.12\,m^3/s$, $D_0 = 7.62\,cm$

$0.24\,m^3/s$, $D_0 = 19.0\,cm$
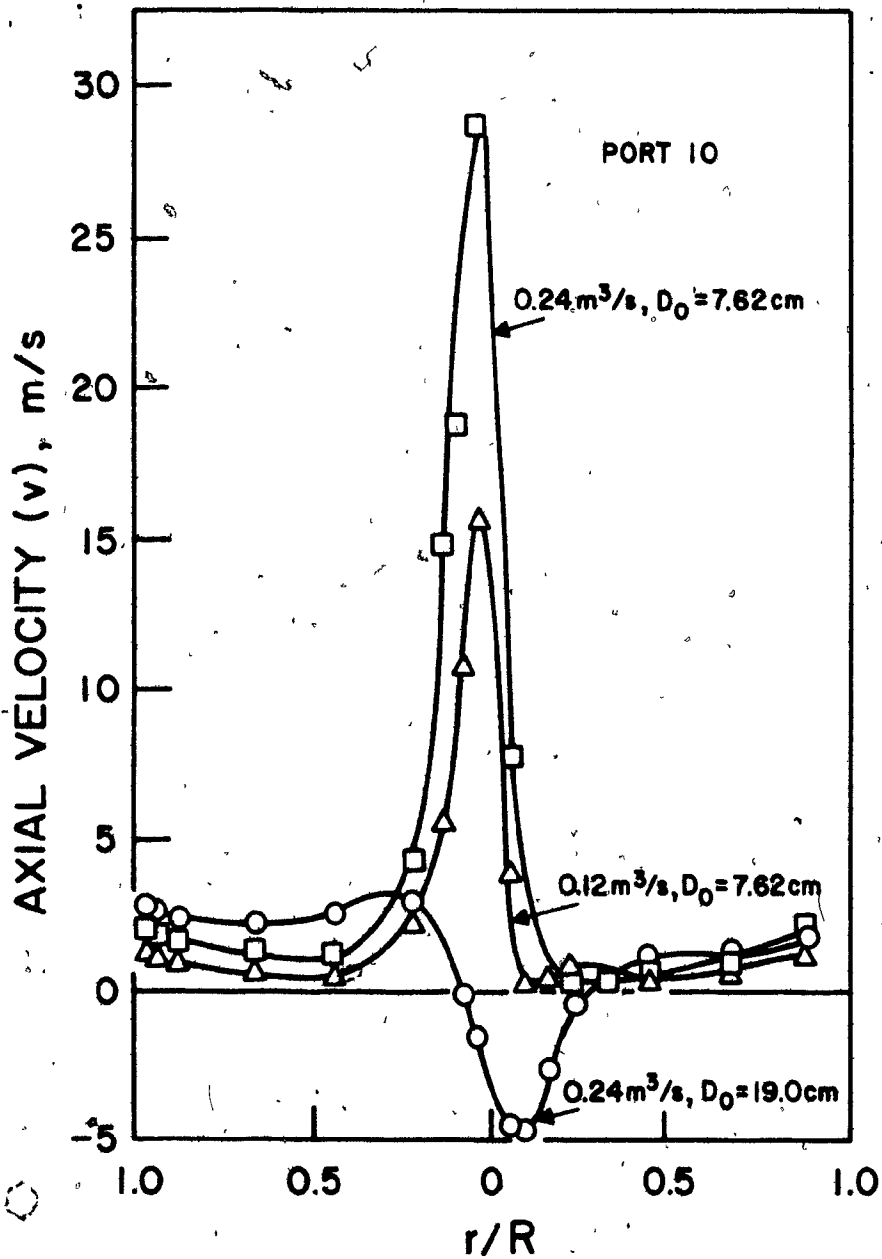
a curve could be obtained for flow rate versus diameters. This
curve would allow the prediction of the onset of backflows in
vortex chambers if the fluid flow rate is varied and one could
avoid them by changing the outlet diameter. This argument still
holds, of course, if the outlet discharges into a duct or other
processing equipment. This would allow for a better working
efficiency for conditions where a backflow is detrimental, such as
in a spray dryer, a cyclone evaporator, a centrifugal absorber,
and in many other types of contacting equipment.

As expected, the effect of the size of the outlet on the
static pressure was shown experimentally to be very large, for the
reasons given above. A typical case is shown in Figure 23. The
static pressure is drastically larger for small outlet diameters
due to the sharp increase in the exit pressure loss (equal to the
value of the kinetic energy in the gas just ahead of the exit).

From these observations, the influence of the sizing of
the outlet diameter on the performance of a vortex flow equipment
becomes quite clear. Needless to say, this influence is also
reflected in the size of the blower required. For example, with
the larger outlet the blower used in this study could deliver up
to 0.6 m³/s, but with the small diameter the capacity was reduced
to a maximum of 0.20 m³/s.

One can also observe from Figure 23 that the dimensionless
radial position where the static pressure becomes equal to the

FIGURE 23

EFFECT OF THE OUTLET DIAMETER (D_0) ON THE

STATIC PRESSURE PROFILES - PORT 10

$Q = 0.24$ m^3/s

INLET VELOCITY = 5 m/s
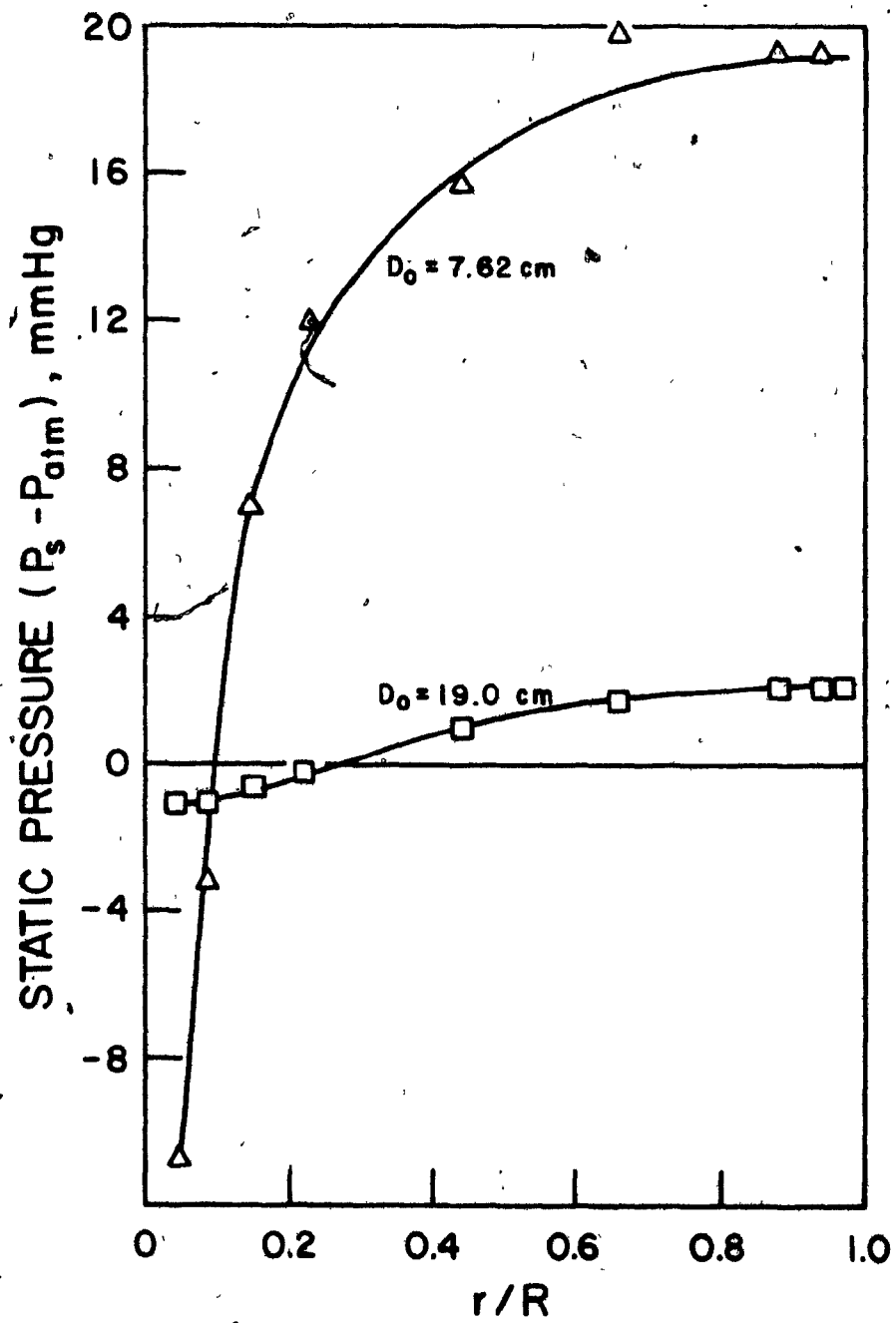
atmospheric pressure also depends on the diameter of the outlet. This figure can be compared with Figure 19 which shows that the static pressure becomes equal to atmospheric pressure at the same radial position for different flow rates.

The tangential velocity profiles were of the same form as the ones obtained with the large diameter outlet. However, the maximum shifted to a position nearer to the centreline of the chamber.

COMPARISON OF THE THEORETICAL MODELS FOR THE TANGENTIAL VELOCITY PROFILES WITH THE EXPERIMENTAL RESULTS

In order to obtain a correlation relating the tangential velocity to the inlet velocity, for any radial and axial position, a computer statistical analysis of the experimental data was performed and multiple regressions gave the desired equations.

For the free-vortex part of the flow, the basis for the multiple regression was Equation (14) derived in the section 'Theoretical Derivation.' This equation is repeated here:

$$w = w_R \ (r/R)^{1-k} \tag{29}$$

This equation was linearized by taking the logarithms of both sides:

$$\log \ (w/w_R) = (1-k) \ \log \ (r/R) \tag{30}$$

For maximum generality, k was taken as being dependent on the entrance velocity, v_0. This is expressed by:

$$k = c_1 (v_0)^n \tag{31}$$

Hence, Equation (30) becomes:

$$\log (w/w_R) = \log (r/R) - c_1 (v_0)^n \log (r/R) \tag{32}$$

At this point a function had to be assumed for w_R. After many trials of curve fittings on the experimental data for w_R the function which gave the best result was found to be:

$$(w_R/v_0) = C_2 (R)^{1-k'} \tag{33}$$

An important conclusion from this result is that the free-vortex tangential velocity profile, extrapolated to positions near the wall, is directly dependent on the radius of the chamber at the particular axial position. No term was needed for other influences of the axial position.

It is now assumed that $k' = k$, for simplification of the equation. This assumption was confirmed later by the perfect fit obtained for the experimental points. Equation (32) now becomes:

$$\log (w/v_0 r) = \log c_2 - c_1 (v_0)^n \log r \tag{34}$$

To obtain the numerical values of c_1, c_2 and n in Equation

(34), a regression analysis was next performed with the aid of a set of statistical programs in the McGill University computing centre. The value of $\underline{n}$ was varied until, for $n = 0$, the best fit was obtained for the hundred experimental data points for various inlet velocities and positions in the chamber. This confirmed that $\underline{k}$ is a constant independent of the flow rate through the chamber or of the inlet velocity to the chamber (see Equation 31) and agrees with the results obtained by other researchers, such as Ogawa (15) and Koval (6). The assumption that $k' = k$ was similarly confirmed. The correlation coefficient obtained was 0.997. The value of $\underline{F}$ was 7361 and the probability associated with $\underline{F}$ was 1.00000.

The constants obtained were:

$$c_1 = 1.72 \text{ and } c_2 = 14.79$$

The final equation for the tangential velocity profile in the free-vortex region is therefore:

$$w = 14.79 \, v_0 \, (r)^{-0.72} \tag{35}$$

From this equation, it can be concluded that the tangential velocity in the free-vortex regions depends only on the inlet velocity and on the radius $\underline{r}$ at the point of interest, and not on the axial position of this point in the chamber (nor on the radius $\underline{R}$ of the cone at the particular axial position). This conclusion is fully supported by Figure 14.

The value of $\underline{k}$ was found to be 1.72. This means that the flow was not a completely developed free-vortex, which would have a $\underline{k}$ value of 2.

It is difficult to compare the value obtained for $\underline{k}$ in this work with the ones reported in the literature because of the differences in set-ups and the difficulty encountered in the measurement of the eddy viscosity. Ogawa (15) shows curves obtained by different authors for the relation (ϵ/ν) versus a Reynolds number defined by:

$$(Re)_0 = W/\rho\nu h \tag{36}$$

From these curves, only a very rough estimate for the eddy kinematic viscosity for our experimental conditions could be deduced because the curves obtained by the different authors differ very much, depending on the type and size of the vortex chamber.

The curve which gave the nearest estimate for the eddy kinematic viscosity at the experimental flow rate conditions used in this study was the one for Ogawa's cyclone. His result was 1.3 g/cm while the value for this study, calculated from the value of $\underline{k}$ and Equation (11), was 2.2 g/cm.

For the forced vortex part of the flow (in the central part of the chamber) Equation (20) was used with a correction to account for the transition to the outer free-vortex region. The modified form of Equation (20) was:

$$w/v_0 = k_1 \, r \exp(-\lambda r) \qquad (37)$$

This was the form which showed the best fit for the experimental data obtained in this study. This form was proposed earlier by Ogawa (15).

For generality, λ was assumed to be of the form:

$$\lambda = -k_2 \, v_0^{\,n} \qquad (38)$$

Substituting (38) in (37):

$$w/v_0 = k_1 \, r \exp[k_2 \, v_0^{\,n} \, r] \qquad (39)$$

This equation was linearized to obtain the constant k_1 and k_2 by regression analyses, while varying the value of n. For $n = -0.17$ the best fit was obtained.

Although the experimental measurements were less accurate in this region, with very steep curves of tangential velocities - versus - dimensionless radius, a correlation coefficient of 0.93 was still obtained.

The final equation for the central part of the flow (forced vortex) was:

$$w/v_0 = 1.03 \, r \exp[-0.153 \, (v_0)^{-0.17} \, r] \qquad (40)$$

Equations (35) and (40) provide a good estimate of the tangential velocity at any position in the vortex chamber.

Figures 24 and 25 show the experimental results for the tangential velocity profiles for different conditions, compared with the curves predicted by Equations (35) and (40).

CONCLUSIONS

It is hoped that the theoretical analysis of the tangential velocity profiles, together with the experimental results on the measurement of the tangential velocity and axial velocity profiles, as well as of the static pressure profiles, which have been presented in this thesis, will contribute to a better understanding of the fluid mechanics of confined vortex flow.

From an experimental point of view, the five-channel pressure probe used in this investigation proved to be more than adequate for the kind of measurements encountered in this work, with the possible exception of the radial velocities, which are so small as to defy all the techniques of measurement known to the author.

The main objective of this research project was to obtain mathematical expressions for the tangential velocity profiles as a function of the inlet air velocity and of the geometry of the system, and in this respect, it can be said that the objective was attained. From a statistical analysis of the experimental data, the predictions of the theoretical analysis based on the Navier-

FIGURE   24

COMPARISON BETWEEN EXPERIMENTAL AND

PREDICTED TANGENTIAL VELOCITY PROFILES – PORT 6

PORT 6
INLET ANGLE =0°

PREDICTED CURVES
FROM CORRELATIONS

EXPERIMENTAL RESULTS
FOR V_o = 12.3 m/s

TANGENTIAL VELOCITY RATIO, w/v_o

RADIAL POSITION, r/R
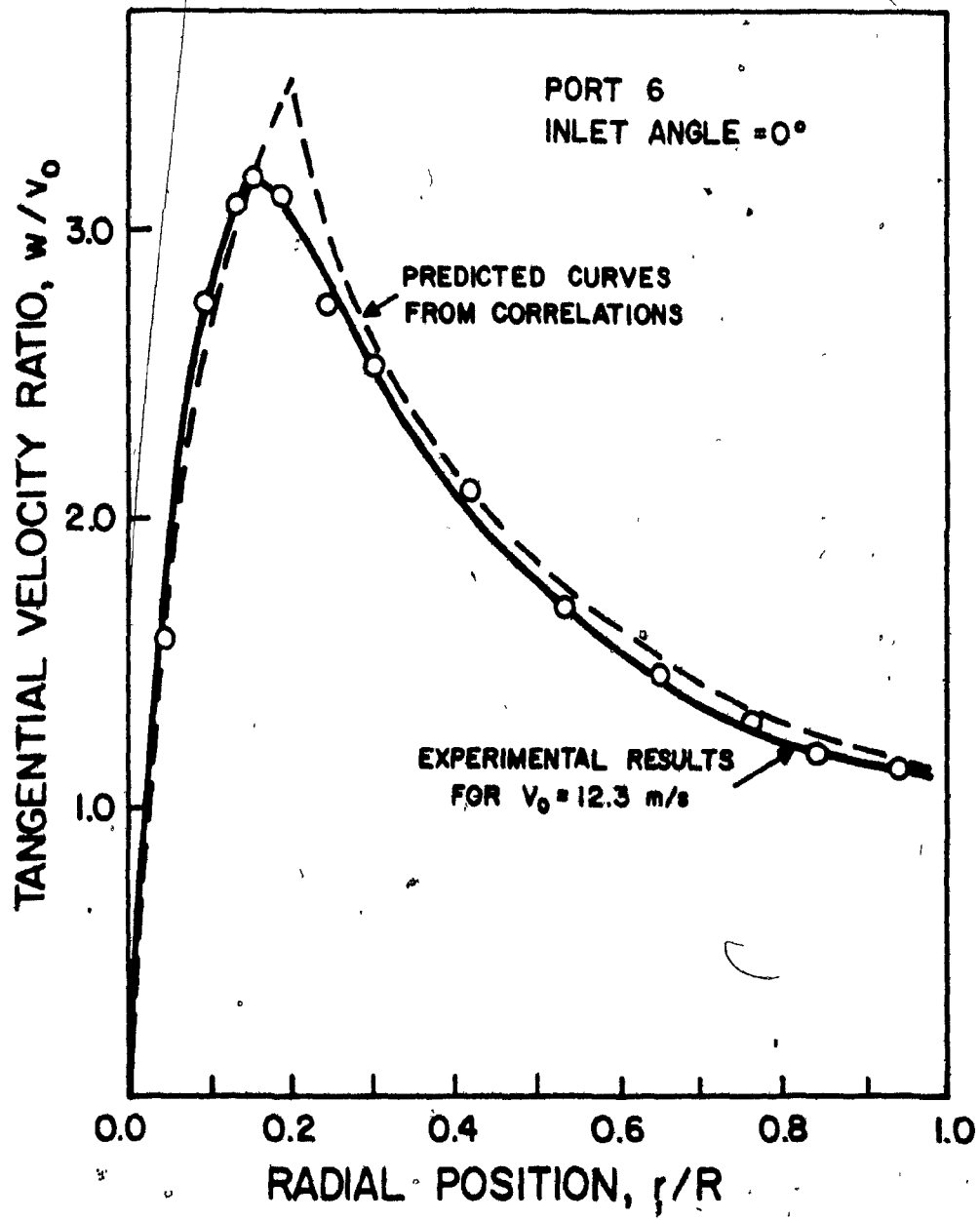
FIGURE   25

COMPARISON BETWEEN EXPERIMENTAL AND PREDICTED

TANGENTIAL VELOCITY PROFILES — PORT 7

PORT 7
INLET ANGLE = 0°

EXPERIMENTAL RESULTS
FOR V_0 = 8.61 m/s

PREDICTED CURVES
FROM CORRELATIONS
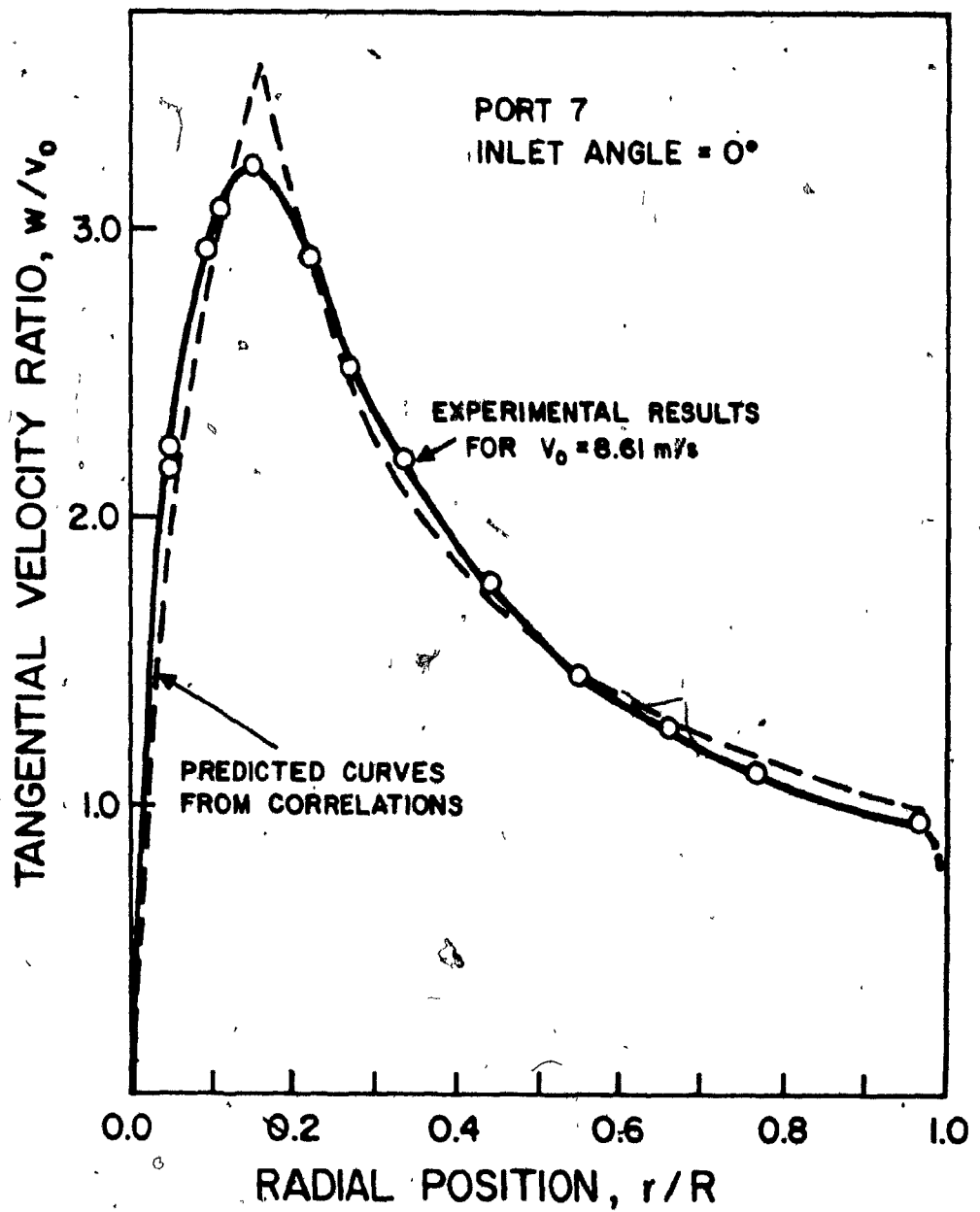
Stokes and on the Continuity equations were fully confirmed in the light of the assumptions that were made in its derivation. It is therefore felt that the forms of the expressions proposed for the two regions of flow have sufficient generality to be applicable to all cylindrical and conical configurations of confined vortex flow. The validity of this statement is further confirmed by the fact that the results of the present study generally agree with the experimental trends and theoretical predictions of other workers in the field. Since tangential velocities are by far the most important characteristic of all equipment in which vortex flows are used, it is felt that this work should have important implications in the design and operation of such equipment.

The discrepancy between the present work and that of Nader Bank (14) is puzzling. Bank used smaller flow rates and a much smaller outlet diameter, which was shown in this study to be conducive to a considerably higher static pressure in the chamber. Also, six inlet ports were used instead of one. Bank's tangential velocity profiles showed a very large forced-vortex portion and a very much smaller free-vortex regime, contrary to the findings of the present study and of other workers in the field. Although the effects of a smaller outlet diameter and of a higher operating static pressure have been examined in a preliminary manner in the present work, more work is obviously required to elucidate the reason for the discrepancy.

The main conclusions of the present study can now be

summarized as follows:

1. The magnitude of the inlet velocity does not change the form of the tangential velocity, axial velocity or static pressure profiles. An increase in inlet velocity increases all these quantities but the forms of the profiles remain the same.

2. The angle of inlet flow has a small effect on the axial velocity profiles, decreasing the symmetry of the flow relative to the axis of the vortex. No effect was observed on the static pressure and tangential velocity profiles.

3. The size of the chamber outlet has very important effects on the operating characteristics of the equipment. With smaller diameter outlets, the possibility of having reverse axial flows decreases and the static pressure levels increase. In addition, the position of maximum tangential velocity approaches the axis of the chamber. There appears to exist a critical outlet diameter size below which no reverse axial flow occurs. This aspect of the work was only examined in a preliminary way, and a more detailed study is indicated.

4. As the diameter of the chamber decreases in the conical section, the free-vortex regime of the tangential velocity profiles decreases in proportion to the total profile.

5. The fluid velocity component in the radial direction is very small and can be neglected for most design purposes.

6. The prediction equations derived in this thesis for
the tangential velocity profiles, which are the most important
characteristic of the flow, can be used directly for equipment
of similar geometries and also for different configurations if
the values of the constants are evaluated. The constant $\underline{k}$ is
the most important parameter for the characterization of the
degree of free-vorticity in the main part of the flow.

NOMENCLATURE

NOMENCLATURE

A	–	Constant
A_1, A_2	–	Constants
C	–	Five-channel probe calibration factor (See Equation 1)
C_1, C_2, C_3, C_4	–	Constants
c_1, c_2, c_3	–	Constants in Equations 31 to 34
D	–	Diameter of 5-channel pressure probe (mm)
D_o	–	Diameter of chamber outlet (cm)
d	–	Diametrical position (cm)
F	–	Probability function
f	–	Total kinematic viscosity $= \nu + \varepsilon$
h	–	Height of chamber at radius r (cm)
K	–	Constant (See Equation 38)
K	–	Five-channel probe calibration factor (See Equation 2)
k_1, k_2	–	Constants (See Equations 37 and 38)
k	–	$W/2\pi \ hf\rho$ (See Equation 11)
k'	–	Constant (See Equation 33)
n	–	General exponent (Equation 31)
P_1	–	Probe's center tapping pressure (mm Hg) (See Figure 8)
$P_2' = (P_2 + P_3)/2$	–	When probe is aligned with flow, i.e., $P_2 = P_3$ (mm Hg)
P_2, P_3, P_4, P_5	–	Probe's side tapping pressures (mm Hg) (See Figure 9)

P_{atm}	–	Atmospheric pressure (mm Hg)
P_c	–	Pressure when the ports of transducer head are interconnected
P_R	–	Pressure R (reference) port of transducer head (mm Hg)
P_S	–	Static pressure (mm Hg)
P_T	–	Total pressure (mm Hg)
P_x	–	Pressure measured on x port of transducer head (mm Hg)
p	–	Pressure (mm Hg)
Q	–	Volumetric flow rate through vortex chamber (m^3/s)
R	–	Radius of chamber at specified horizontal section (cm)
r	–	Radius (cm)
Re_0	–	Reynolds number defined by Equation 37
$(Re)_D$	–	Reynolds number based on external diameter of probe
$(Re)_d$	–	Reynolds number based on tapping diameter for probe
$(Re)_r$	–	Reynolds number based on radial position in chamber and radial velocity $= ur/\nu$
R_0	–	Radius of chamber's outlet (cm)
T	–	Absolute temperature ($^\circ$K)
u	–	Radial velocity (cylindrical coordinates) (m/s)
V	–	Velocity vector intensity (m/s)
v	–	Axial velocity (cylindrical coordinates) (m/s)
v_0	–	Entrance velocity (m/s)
W	–	Mass flow rate entering the chamber (g/s)

w   – Tangential component of velocity (cylindrical coordinates) (m/s)

w_R – Tangential velocity at radius R (m/s)

z   – Height in chamber (measured from the top) (cm)

Greek Letters

ϵ – Eddy kinematic viscosity (cm²/s)

λ – Constant (See Equation 38)

ν – Fluid kinematic viscosity (cm²/s)

Ω_z – Vorticity (z component)

ψ – Angle of flow relative to a horizontal plane (°)

ρ – Fluid density (g/cm³)

θ – Pitch angle (degrees)

BIBLIOGRAPHY

BIBLIOGRAPHY

1. Gauvin, W.H., Katta, S. and Knelman, F.H., 'Drop Trajectory Predictions and Their Importance in the Design of Spray Dryers', Int. J. Multiphase Flow, 1, (1975), 793.

2. Katta, S. and Gauvin, W.H., 'Some Fundamental Aspects of Spray Drying', A.I.Ch.E. Journal, 21, 1, (1975), 143.

3. Bank, N. and Gauvin, W.H., 'Measurements of Flow Characteristics in a Confined Vortex Flow', Can. J. Chem. Eng., 55 (1977), 397.

4. Perry, J.H., 'Chemical Engineers' Handbook', McGraw Hill Book Co., 4th ed.

5. Mensing, A.E., et al. 'Investigation of the Use of a Vortex Flow to Separate Oil from an Oil-Water Mixture', United Aircraft-Research Laboratories, Report 714/03/A/001, (Nov. 1970).

6. Koval, V.P. and Mikhailov, S.L., 'Velocity and Pressure Distribution of Liquid in a Swirl Chamber', Teploenergetika, vol. 19, no. 2, (1972), 25-28.

7. Syred, N. and Beer, J.M. 'Combustion in Swirling Flows: A Review', Combustion and Flame, vol. 23, (1974), 143-201.

8. Baddour, R.F. and Timmins, R.S., 'The Application of Plasmas to Chemical Processing', MIT Press, 1967.

9. Gardeman, D.A. and Hecht, N.L., 'Arc Plasma Technology in Material Science', Springer-Verlag, 1972.

10. Pfender, E., 'Generation of an Almost Fully Ionized, Spectrally Clean, High Density Hydrogen Plasma', Proceedings of the 6th International Conference on Ionization Phenomena in Gases, edited by P. Hubert and E. Cremieu - Alcan, (Paris, 1963), vol. II, pp 369-374.

11. Baluev, E.D. and Troyankin, Yu. V., 'The Aerodynamic Resistance and Efficiency of a Cyclone Chamber', Teploenergetika, vol. 16, no. 6, (1969), 29.

12. Baluev, E.D. and Troyankin, Yu. V., 'Study of the Aerodynamic Structure of Gas Flow in a Cyclone Chamber', Teploenergetika, vol. 14, no. 1, (1967), 63-65.

13. Baluev, E.D. and Troyankin, Yu. V., 'The Effect of the Design Parameters on the Aerodynamics of Cyclone Chambers', Teploenergetika, vol. 14, no. 2, (1967), 67-71.

14. Bank, N., 'Measurements of Flow Characteristics in a Confined Vortex Flow', M. Eng. Thesis, Department of Chemical Engineering, McGill University, (1975).

15. Ogawa, A., 'On the flow Pattern of the Turbulent Rotational Flow in the Returned Type of the Vortex Chamber', J. Coll. Engng. Nihon Univ., Series A, 17, (1976), 51.

16. Marshall, W.R., Jr., 'Atomization and Spray Drying', Chem. Eng. Progress Monograph Series, vol. 50, no. 2, (1954).

17. Rietema, K. and Krajenbrink, H.J., 'Theoretical Derivation of Tangential Velocity Profiles in a Flat Vortex Chamber - Influence of Turbulence and Wall Friction', Appl. Sci. Res., vol. 8, Section A, (1958).

18. Chigier, N.A., 'Velocity Measurement in Vortex Flows', A.S.M.E. Paper no. 5-1-31, (May 1971).

19. Kendall, J.M., Jr., 'Experimental Study of a Compressible Viscous Vortex', J.P.L. Rep. TR 32-290, (1962).

20. Schowalter, W.R. and Johnstone, H.F., 'Characteristics of the Mean Flow Patterns and Structure of Turbulence in Spiral Gas Streams', A.I.Ch.E. Journal, vol. 6, no. 4, (1960), 649.

21. Bank, N. and Gauvin, W.H., 'Inclined Hot-Wire Response Equations for a Flow Field Having a Dominant Tangential Velocity Component', Can. J. Chem. Eng., 55, (1977), 516.

22. Yuan, S.W., 'Foundations of Fluid Mechanics', Prentice Hall, Toronto (1967).

23. United Sensor and Control Corp., 'Pitot-Static Pressure Process', Bulletin 1, (1977).

24. Chue, S.H., 'Pressure Probes for Fluid Measurement', Prog. Aerospace Sci., vol. 16, no. 2, (1975), 147.

25. United Sensor and Control Corp., 'Traversing Probe Errors', Technical Bulletin T-1 (1977).

26. United Sensor and Control Corp., 'Theory and Application of Fluid Flow Probes', Technical Bulletin T-2 (1977).

27. Murphy, I.D., Jr., 'Design and Analysis of Industrial Experiments', Chemical Engineering, vol. 84, no. 12, (1977), 168.

APPENDIX

METHOD OF CALCULATION OF VELOCITY COMPONENTS AND STATIC PRESSURES
FROM THE FIVE-CHANNEL PRESSURE PROBE READINGS

The method described below was developed for the programable calculator HP-25C manufactured by Hewlett Packard Company. It is based on Equations (22) to (27) of the Experimental Section.

This program calculates the values of $(P_T - P_S)$, $(P_S - P_{atm})$, Θ, $\underline{V}$, $\underline{w}$, and $\underline{v}$, in mm Hg, degrees, and m/s, respectively. The parameters needed as input are P_{atm}, $(P_4 - P_5)$, $(P_1 - P_2)$, $(P_1 - P_{atm})$ $\underline{T}$, and $\underline{\Psi}$, given in mm Hg, °C, and degrees, respectively. In these experiments these parameters were measured with the five-channel pressure probe as explained in the section Operating Procedures. The probe's calibration curves (see Figure 6) were used to obtain intermediate factors used in the calculations.

The program steps are presented below:

LINE	CODE	KEY ENTRY	
00			
01	24 01	RCL	1
02	71	÷	
03	74	R/S	
04	24 01	RCL	1
05	24 04	RCL	4

LINE	CODE	KEY ENTRY	
06	61		x
07	74	R/S	
08	23 06	STO	6
09	24 05	RCL	5
10	61		x
11	24 06	RCL	6
12	51		+
13	24 02	RCL	2
14	41		-
15	32	CHS	
16	74	R/S	
17	23 51 00	STO + 0	
18	24 03	RCL	3
19 to 24		273.15	
25	51		+
26	24 00	RCL	0
27	71		÷
28	24 06	RCL	6
29	61		x
30	14 02	f√x	
31	24 07	RCL	7
32	61		x
33	74	R/S	
34	22		↓R

LINE	CODE	KEY ENTRY
35	21	$x \not\gtrless y$
36	14 09	$f \rightarrow R$
37	21	$x \not\gtrless y$
38	22	$\downarrow R$
39	21	$x \not\gtrless y$
40	22	$\downarrow R$
41	14 09	$f \rightarrow R$
42	74	R/S
43	22	$\downarrow R$
44	74	R/S
45	22	$\downarrow R$
46	74	R/S
47	13 00	GTO 00

Instructions for the uses of the program after it was keyed in were:

INPUT DATA	KEYS	OUTPUT
P_{atm}	STO 0	
(P_1-P_2)	STO 1	
(P_1-P_{atm})	STO 2	
T	STO 3	
23.94	STO 7	
	f PROGM	
(P_4-P_5)	R/S	$(P_4-P_5)/(P_1-P_2)$

At this stage, a value for $(P_4 - P_5)/(P_1 - P_2)$ was displayed. For this value, $\underline{\theta}$, $\underline{K}$ and $\underline{F}$ were read from the probe's calibration curve. Now, the instructions below were followed:

INPUT DATA	KEYS	OUTPUT
K	STO 4	
F	STO 5	
	R/S	$(P_T - P_S)$
	R/S	$(P_S - P_{atm})$
	R/S	V
θ	ENTER	
ψ	R/S	w
	R/S	v
	R/S	u

In the present case there were inaccuracies in the measurement of $\underline{\theta}$ which hampered the reliability of the calculation of $\underline{u}$, which is the component dependent on this angle. So, this component was not calculated. But this program is shown in a complete form and can be used in any case where a five-channel pressure probe is used for flow characteristic measurements in air.